Robotica (2010) volume 28, pp. 689–703. © Cambridge University Press 2009
doi:10.1017/S0263574709990336

# To enhance transparency of a piezo-actuated tele-micromanipulator using passive bilateral control

R. Seifabadi†,‡,* , S. M. Rezaei†,‡, S. Shiry Ghidary†,§, M. Zareinejad†,‡, M. Saadat¶

†*New Technologies Research Centre (NTRC), Amirkabir University of Technology, Tehran, Iran*
‡*Mechnical Engineering Department, Amirkabir University of Technology, Tehran, Iran*
§*Computer Engineering Department, Amirkabir University of Technology, Tehran, Iran*
¶*Mechnical Engineering Department, University of Birmingham, Birmingham, UK*

(Received in Final Form: July 23, 2009. First published online: August 27, 2009)

## SUMMARY

This paper presents the research work on a 1 degree of freedom (DOF) force reflecting tele-micromanipulation system. This system enables a human operator to position remote objects very precisely having haptic feedback. The slave robot is a nano-positioning piezo-actuator with hysteretic dynamics. This intrinsic nonlinearity results in positioning inaccuracy and instability. Hence, a LuGre friction model is employed to model and compensate for this undesirable behavior. By means of a transformation, the 2-DOF master–slave system (1-DOF each) is decomposed into two 1-DOF new systems: the shape system, representing the master–slave position coordination, and the locked system, representing dynamics of the coordinated system. A key innovation of this paper is to generalize this approach to the hysteresis-type nonlinear teleoperated systems. For the shape system, a position tracking controller is designed in order to achieve position coordination. This position coordination is guaranteed not only in free space motion, but also during contact at the slave side. Furthermore, a force tracking controller is designed for the locked system in order to achieve tracking of the force exerted on the master and slave robots. Using this force controller, transparency is remarkably enhanced. Based on the virtual flywheels concept, passivity of the closed-loop teleoperator is guaranteed against dynamic parameter uncertainties and force measurement inaccuracies. The simulation and experimental results verify the capability of the proposed control architectures in achieving high-level tracking of the position and force signals while the system remains stable.

KEYWORDS: Macro–micro teleoperation; Piezo-actuator; Hysteresis nonlinearity; LuGre friction model; Position and force tracking; Decomposition; Shape and locked systems; Virtual flywheel; Passivity; Scaling.

## 1. Introduction

Micromanipulation has been attracting growing interest in recent years. There are many applications in which slave environment is in micrometer dimensions. The operation complexity may urge a human operator to be present in the control loop. The human operator interacts with a macro-scaled master robot, say a joystick, whereas the slave robot interacts with a micro-scaled environment. Micro-assembly[1] and in vitro fertilization[2] are two common examples of such systems. To achieve accurate positioning in these applications, interest has been taken in piezo-actuators because of their ability in achieving high-precision positioning.[3]

In this research, a 1 degree of freedom (DOF) bilateral macro–micro teleoperation system has been developed. An application of this micromanipulator is to guide a needle insertion device to intervene into very tiny organs like the retina. To achieve force control for a human operator and consequently increase the chance of doing a successful task, this system should be bilateral (i.e. have a force feedback from the slave environment). To accomplish micro-positioning, in this work a piezo-actuator was used as the slave robot. The most important drawback of piezo-actuators is their nonlinear hysteretic dynamics which results in positioning inaccuracy and instability. Generally, to compensate for the hysteresis effect in control systems, an established model or function that can accurately represent the hysteresis feature is very important.[4] Therefore, many methods have been proposed in recent years to cope with this undesirable effect.[5–9] Here, the LuGre friction function model is used as the estimator of the hysteresis effect. The idea to use a friction model to estimate the hysteresis effect was proposed by Shieh *et al.* in refs. [4], [10], and [11]. They mention so many advantages of this model in comparison with the previous methods.[4]

Two fundamental objectives of a teleoperation system are achieving maximum transparency (telepresence) while keeping stability. To define transparency, two alternative approaches have been proposed: one proposes impedance, that is, how transmitted impedance (i.e. human force/master velocity) is equal to environmental impedance (i.e. environmental force/slave velocity).[12] The other approach proposes simultaneous tracking of position and the force exerted on the two robots as a measure of transparency,[13]

* Corresponding author. E-mail: reza.seifabadi@queensu.ca

which fits well into the 1-DOF teleoperated systems. In this research, the second approach has been used.

By means of a transformation, the master–slave system is decomposed into two new subsystems: the shape system representing the master–slave position coordination (i.e. position tracking) and the locked system representing the dynamics of the coordinated system (i.e. after position tracking happens). The idea of this transformation was primarily proposed in ref. [14] for a pair of macro-scaled dynamically similar $2n$-DOF linear system, and then developed for macro-scaled $2n$-DOF nonlinear systems.[15] In the latter research, the nonlinearity pertained to the nonunity degree of freedom. As a result of this nonintrinsic nonlinearity, tremendous simplicity was achieved during both control design and stabilization. However, the nonlinearity of the slave robot used in this research is intrinsic, belonging to the hysteretic nature of piezo-actuators. For that reason, approximately all theorems, lemmas, propositions, and equations provided in refs. [15] and [16] must be reestablished when applied to the current teleoperator. Therefore, the main contribution of this paper is to make this powerful approach applicable to hysteresis-type nonlinear teleoperated systems.

To achieve position tracking, a modified Propotional-Derivative (PD) controller is designed for the shape system (the system responsible for position coordination). This controller accounts for position tracking not only in free space motion ($F_1 = F_2 = 0$), but also during micro-positioning (that is, during contact between the slave and environment ($F_1$ and $F_2 \neq 0$)).

To ensure tracking of the force exerted on the master and slave robots, an impedance controller was designed for the locked system. The locked system controller used in refs. [15] and [16] was a simple inertia scaling controller that aimed only to induce a desired inertia to the locked system. In fact, in these works, there was no evidence of force tracking. The current impedance controller, however, achieves acceptable force tracking. Therefore, transparency of the current teleoperation system is enhanced remarkably when compared with previous works.

To keep the closed-loop teleoperation system passive against dynamic parameter uncertainty and force measurement inaccuracy, some approaches have been reported. In our previous work,[17] a sliding-mode-based controller was used to overcome dynamic parameter uncertainty and unknown but bounded time delay for the same tele-micromanipulation setup. Reference [18] proposes the use of an $H_\infty$ loop-shaping approach to tradeoff the robustness and uncertainties in environment models for a prespecified time delayed tele-micromanipulation system. Here, the shape and locked system controllers (i.e. position and force tracking controller) are established in a negative semi-definite (NSD) structure. Within this NSD structure, there are some troublesome terms (i.e. terms that may endanger passivity of the controllers). To resolve this issue, the virtual flywheels concept has been employed.[19] According to this concept, the energy generated by these terms can be taken out of some virtual flywheels with bounded kinetic energy deposited on them. That means the energy generated by the controllers never exceeds these boundaries, and consequently the system always remains stable.

In this paper, time delay in communication channels is supposed to be negligible. This assumption originates from the fact that the master and slave robots are sufficiently close to each other. In addition, the sampling rate of the whole experimental setup is adequately high. The experimental results in Section 10 will confirm this technical assumption.

In this research, all dynamic parameters are supposed to include uncertainty, in particular the LuGre dynamic parameters, since the LuGre model does not take load dependency into account, and consequently is insensitive to the environmental force. Therefore, the control framework must have satisfactory robustness against these uncertainties. In Section 7, it can be observed that arranging the control architecture in an NSD structure fulfills this objective.

This paper is organized as follows. Section 2 introduces the experimental setup. In Section 3, the modeling and identification of teleoperators are considered. In Section 4, the problem is defined and the control objectives are introduced. In Section 5, the system is decomposed into the locked and shape systems. Section 6 discusses the designs for the locked and shape controllers to satisfy the objectives. In Section 7, the passivity of the system is discussed. Sections 8, 9, and 10 include the parameters design, simulation, and experimental results, respectively. The paper ends with the conclusions and some future work remarks in Section 11.

## 2. Experimental Setup

Figure 1 shows the experimental setup. A servo DC motor (Fig. 1, No. 6) has been used as the master robot to match the 1-DOF slave robot. This servo DC motor has a nominal power of 120 W, producing a sufficiently large torque (max. 0.3 Nm in 4.5 A) on the operator's hand during hard contact. The DC motor is equipped with a differential encoder (with a resolution of 0.5°). A DC motor driver is used (Fig. 1, No. 14) to amplify the master control signal. A 2-kg loadcell is used as the master force sensor while a 1-kg loadcell is used as the slave force sensor. Figure 2 shows how the force sensors are being oriented with respect to the robots. The slave robot used in this research is a Compact X Piezoelectric Nanopositioning System PI 611.1S (Fig. 2b, No. 1), the maximum displacement of which is 100 μm and its smallest step 0.1 nm.

A data acquisition board (DAB) has been used. This DAB has three distinct roles within the experimental setup: (1) It acts as an interface between the hardware (i.e. robots) and the software (i.e. controllers all produced in PC); (2) it produces real-time control signals from the controller signals built in MATLAB/Simulink; and (3) it provides a peripheral software which enables us to monitor position and force signals, and tuning control gains during operation without going to Simulink files.

The output signals of the force sensors are amplified by use of two amplifiers with a gain of 10,000 (Fig. 1, Nos. 10 and 11). To have a visual feedback from the microenvironment, a three-eye stereo zoom microscope (loop) has been used (Fig. 1, No. 2). The microscope was equipped with a CCD camera. The maximum magnification of the microscope and

https://doi.org/10.1017/S0263574709990336 Published online by Cambridge University Press

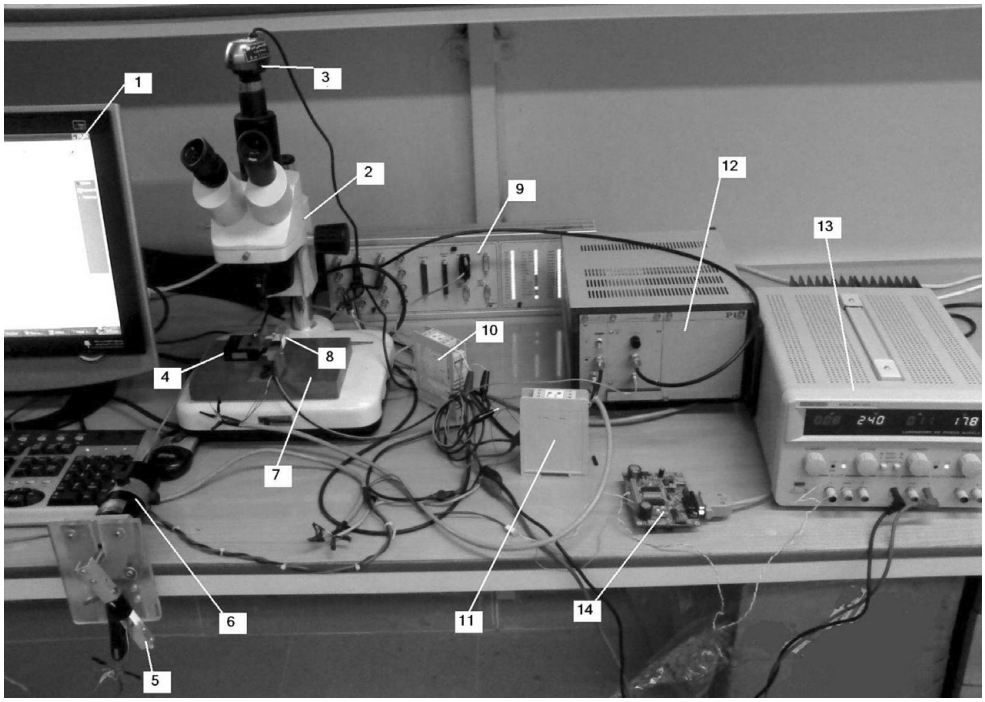


Fig. 1. Bilateral macro–micro telemanipulation experimental setup used in this research: (1) PC, (2) stereo zoom microscope (max. 90×), (3) CCD camera with a 16× magnification, (4) slave robot (nanopositioning piezo actuator), (5) master force sensor, (6) master robot (a servo DC motor), (7) chassis for the slave and its force sensor, (8) force sensor at the slave side, (9) connecter panel of the data acquisition board, (10) master force sensor amplifier, (11) slave force sensor amplifier, (12) slave robot driver and its position sensor amplifier, (13) power supply, and (14) DC motor driver (Roboteq).

the camera together is 384×. The control program is designed in MATLAB 7.1/Simulink, which afterward will be compiled into the C program (by the DAB processor). A PC (Fig. 1, No. 1) is also used. This PC serves to produce highly sophisticated control commands (e.g. hysteresis compensator) as well as provides an online signal monitoring and visual feedback from the micro-scaled environment. Finally, a power supply is used (Fig. 1, No. 13) to supply the master robot and the force sensor amplifiers.

## 3. Modeling and Identification of the System

### *3.1. Modeling of the master robot*

The transfer function (angular velocity over the input voltage) for the master robot in the Laplace domain is as follows[20]:

$$
\begin{aligned}
G_{\mathrm{m}}(s) &= \frac{\omega(s)}{V(s)} = \frac{1/K_{\mathrm{E}}}{(s\tau_{\mathrm{m}}+1)(s\tau_{\mathrm{e}}+1)} \\
\tau_{\mathrm{m}} &= \frac{RJ_{\theta}}{K_{\mathrm{E}}K_{\mathrm{T}}} := \text{Mechanical time constant}, \\
\tau_{\mathrm{e}} &= \frac{L_{\mathrm{a}}}{R} := \text{Electrical time constant}
\end{aligned}
\tag{1}
$$

where $V$ (in volt) is the motor input voltage (= master control signal), $R$ (in Ω) and $L_a$ (in H) are the resistance and inductance of the armature, $\omega$ (in rad/s) is the angular velocity, $J_\theta$ (kg m$^2$) is the moment of inertia of the rotor, encoder, or whatever connected to it (here, the master force sensor, Fig. 2a), $B_\theta$ is the viscous damping factor of the motor, $K_{\mathrm{E}}$ (in V s/rad) and $K_T$ (in Nm/A) are the voltage and

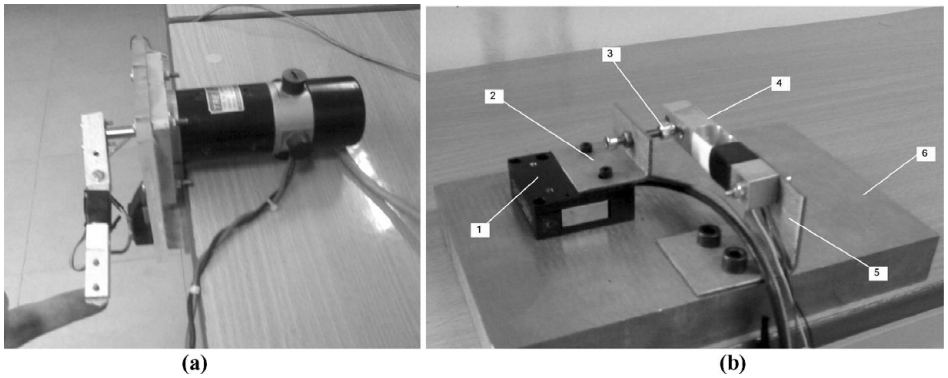


(a) (b)

Fig. 2. Close-up views of the master and slave robots: (a) Master force sensor linked to the master robot; (b) The slave robot: (1) slave robot (nanopositioning piezo actuator), (2) holder of the end effecter, (3) end effecter, (4) slave force sensor, (5) loadcell holder, (6) platform.

https://doi.org/10.1017/S0263574709990336 Published online by Cambridge University Press

Table I. Identified master dynamic parameters.

| $J_\theta$ (kg m$^2$) | $B_\theta$ (Ns/m) | $K$ (N/V) | $L_{\text{eff}}$ (m) | $a$ (s$^{-1}$) | $k$ (v$^{-1}$s$^{-2}$) |
|---|---|---|---|---|---|
| $0.35 \times 10^{-4}$ | 0.0023 | 0.0227 | 0.15 | 67 | 648.1 |

torque constants of the motor, respectively, and $s$ denotes the Laplace domain variable.

For the servo DC motor, the mechanical time constant is much larger than the electrical time constant. Therefore, the second-order transfer function of Eq. (1) would be simplified to a first-order system:

$$G_{\text{m}}(s) = \frac{1/K_{\text{E}}}{(s\tau_{\text{m}} + 1)} = \frac{k}{s + a}, \tag{2}$$

where $k = 1/(K_{\text{E}}\tau_{\text{m}})$ and $\alpha = 1/\tau_{\text{m}}$. Equation 2 can be rewritten in time domain:

$$\frac{\text{d}\omega}{\text{d}t} = -a\omega - kv. \tag{3}$$

Also, Newton's second law for the servo DC motor will result in the following:

$$J_\theta \frac{\text{d}\omega}{\text{d}t} + B_\theta\omega = Kv + F_1.L_{\text{eff}} \Leftrightarrow J_\theta\ddot{\theta}(t) + B_\theta\dot{\theta}(t) = \underbrace{Kv}_{T_1.L_{\text{eff}}} + F_1.L_{\text{eff}}z, \tag{4}$$

where $K$ is the voltage-to-torque factor, $F_1$ is the force exerted by the human operator on the master robot, $L_{\text{eff}}$ is the effective arm of exerting $F_1$, and $T_1(N)$ is the master control signal.

Comparing Eqs. (3) and (4), it can be concluded that $B_\theta = \alpha J_\theta$ and $K = kJ_\theta$.

### 3.2. Identification of the master robot

The values of the master dynamic parameters can be achieved easily by applying a step input of 24 V to the servo DC motor and analyzing the response of the system to that input. The results are listed in Table I.

### 3.3. Modeling of the slave robot

The LuGre model, originally a friction model,[21] has been employed to model the hysteresis effect in piezo-actuators because, mathematically, this model establishes a hysteretic input–output mapping.[4] The key advantage of this model is that it can produce the term compensating for the hysteresis effect in control signal more rapidly and accurately.[4,10,11] In addition, there are still two important reasons why the LuGre friction model is used in this research: (1) As will be discussed later, the LuGre model is added as a feedback to the linear part of the slave dynamics. This feedback structure makes the hysteresis compensation easier, and (2) this model is well sensitive to the frequency of the input signal, according to our observations. In other words, the LuGre model is a frequency-dependent model. This is rather important because the human operator may command the master (and consequently the slave) with different frequencies, which could result in positioning inaccuracy and/or instability if the model used did not account for changes in frequency.

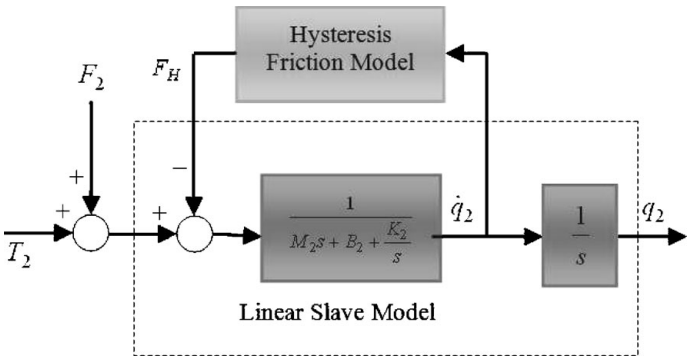


Fig. 3. Slave robot complete block diagram. The hysteresis effect has been added as a feedback to the linear dynamics.

The complete block diagram of the slave robot is depicted in Fig. 3. The hysteresis effect has been added as a feedback to the linear dynamics:

$$M_2\ddot{q}_2(t) + B_2\dot{q}_2(t) + K_2q_2(t) + F_{\text{H}} = \underbrace{K'.v}_{T_2} + F_2, \tag{5}$$

where $M_2$, $B_2$, and $K_2$ are the inertia, viscous damping, and equivalent stiffness of the slave robot, respectively. $q_2$ is the position of the slave, $K'$ is the voltage-to-force factor, $v$ is the slave input voltage, $F_2$ is the environmental force, and $T_2(N)$ is the slave robot control signal. $F_{\text{H}}$, the LuGre friction function, can be achieved from the following set of equations[4]:

$$\begin{cases} \dot{z}(t) = \dot{q}_2 - \sigma_0 \dfrac{|\dot{q}_2|}{g(\dot{q}_2)} z \\ g(\dot{q}_2) = F_{\text{C}} + (F_{\text{S}} - F_{\text{C}})\text{e}^{-(\dot{q}_2/v_{\text{St}})^2}. \\ F_{\text{H}} = \sigma_0 z + \sigma_1\dot{z}(t) + \sigma_2\dot{q}_2 \end{cases} \tag{6}$$

Here $\sigma_0, \sigma_1, \sigma_2, F_{\text{C}}, F_{\text{S}}$, and $v_{\text{St}}$ are constants. For more details about the LuGre friction model, please refer to refs. [21] and [22].

### 3.4. Identification of the slave robot

The slave robot dynamics defined in Eq. (5) comprises two subsystems: a linear dynamics represented by $M_2$, $B_2$, $K_2$, and $K'$, and a nonlinear dynamics represented by $\sigma_0$, $\sigma_1$, $\sigma_2$, $F_{\text{C}}$, $F_{\text{S}}$, and $v_{\text{St}}$. Therefore, the identification of the slave robot will have two stages: the linear part identification and the nonlinear dynamics identification.

*3.4.1. Identification of the linear dynamics.* At first glance, a step input does not seem to be a suitable input to identify linear dynamics, since the slave dynamics has hysteresis nonlinearity. But, it can still be the appropriate input if the nonlinear term, $F_{\text{H}}$, remains unchanged (set to zero) for any step input. To verify that, the following method is proposed:

A successful method of hysteresis modeling and compensation in piezo-actuators is the Prandtl–Ishlinskii method.[23] If the corresponding Prandtl–Ishlinskii inverse dynamics of the slave does not change the step input, it

https://doi.org/10.1017/S0263574709990336 Published online by Cambridge University Press

Table II. Identified slave linear dynamic parameters.

| $K'$ (N/V) | $\zeta$ | $\omega_n$ (rad/s) | $M_2$ (kg) | $B_2$ (Ns/m) | $K_2$ (N/m) |
|---|---|---|---|---|---|
| 0.2194 | 0.8301 | 497.087 | 2.17 | 1078.67 | $3.0 \times 10^5$ |

can be concluded that the nonlinear term $F_H$ would be insensitive to the step input, and consequently the step input can be an appropriate candidate to identify the linear part. Experimental results revealed that the output of the Prandtl–Ishlinskii inverse dynamics of the slave for an arbitrary step input remains unchanged.[24] That means a step input is a suitable candidate. Details on the Prandtl–Ishlinskii model and its inverse dynamics are discussed in refs. [24], [25], and the references therein.

The slave robot response to step input revealed that the slave is an overdamped (i.e. without overshot) second-order system. To identify linear parameter dynamics of a second-order system using a step input, an overshot is required. To achieve this, the slave open loop is temporarily closed by a simple proportional controller ($P = 1.031$). Response of the closed-loop system was plotted for a step input of $v_0 = 52$ V. From the overshot (% M) and rise time ($t_r$), dimensionless viscous damping ratio ($\zeta$) and undamped natural frequency ($\omega_n$) were determined. Steady-state response (output final value) provides the third equation. $K_2$ is known form data sheet. Therefore, the number of equations and unknown parameters become identical. The result of this identification is provided in Table II.

*3.4.2. Identification of the nonlinear dynamics.* To identify nonlinear dynamic parameters (i.e. LuGre parameters), some algorithms have been reported.[22,26,27] However, these methods are effective as far as the LuGre model is modeling friction between two sliding surfaces, but these are unfortunately inapplicable when the LuGre model is representing a hysteresis feature.[28] Therefore, trial and error seems to be the only option to find LuGre dynamic parameters.

To find $\sigma_0$, $\sigma_1$, $\sigma_2$, $F_C$, $F_S$, and $v_{St}$, an experiment was conducted on the slave robot: a sinusoidal voltage with an amplitude of $v_0 = 10$ V and a frequency of 1 Hz was fed to the slave robot. The slave output signal (i.e. position) was then plotted versus the input signal (i.e. voltage). This resulted in a hysteresis loop (Fig. 4, outer loop). Then, the LuGre dynamic parameters were tuned such that the model fit satisfactorily on the loop gained from the experiment. While tuning, the following results were achieved: the height of the loop decreases as $\sigma_0$ increases (the LuGre model rotates clockwise). The thickness of the loop (LuGre model) increases as either of $\sigma_1$ or $\sigma_2$ increases. $F_C$, $F_S$, and $v_{St}$ cause no tangible change in the loop shape. Now, it would be easy to fit the model on the experiment by a quick trial and error (Fig. 4). The result of this identification is shown in Table III.

*3.5. Position and force scaling*

Macro-scaled position/velocity signals of the master robot should be scaled down beyond the communication channels to drive the slave robot which moves in micrometer

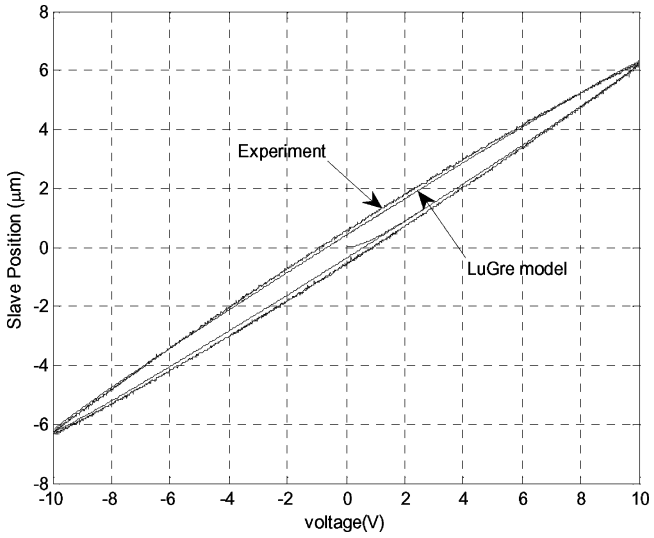


Fig. 4. LuGre model fits well on the experiment at the end of the identification process.

Table III. Identified slave nonlinear dynamic parameters.

| $\sigma_0$ (N/m) | $\sigma_1$ (Ns/m) | $\sigma_2$ (Ns/m) | $F_C$ (N) | $F_s$ (N) | $v_{St}$ (m/s) |
|---|---|---|---|---|---|
| $0.5 \times 10^5$ | $0.8 \times 10^3$ | $2 \times 10^4$ | 7 | 10 | 45 |

dimensions. On the contrary, small environmental force should be scaled up such that the human operator can sense environmental contact. Due to the presence of the nonlinear term $F_H$ in slave dynamics, both position and force scaling factors were applied to the master model. First, the position scaling factor $k_p$ is inserted as follows:

$$\begin{aligned}(4) &\Rightarrow \frac{J_\theta}{L_{\text{eff}}^2}(L_{\text{eff}}\ddot{\theta}) + \frac{B_\theta}{L_{\text{eff}}^2}(L_{\text{eff}}\dot{\theta}) = T_1 + F_1 \\ &\Rightarrow \frac{J_\theta}{L_{\text{eff}}^2}\ddot{q}_1 + \frac{B_\theta}{L_{\text{eff}}^2}\dot{q}_1 = T_1 + F_1 \\ &\Rightarrow \frac{J_\theta}{k_p L_{\text{eff}}^2}(\underbrace{k_p\ddot{q}_1}_{\ddot{Q}_1}) + \frac{B_\theta}{k_p L_{\text{eff}}^2}(\underbrace{k_p\dot{q}_1}_{\dot{Q}_1}) = T_1 + F_1\end{aligned}, \quad (7)$$

where $q_1 = L_{\text{eff}}\,\theta$ and $Q_1 = k_p q_1$. Then, the force scaling factor $k_f$ is inserted into Eq. (7):

$$\frac{1}{k_f}[M_1\ddot{Q}_1 + B_1\dot{Q}_1 = T_1 + F_1], \quad (8)$$

where $M_1 = J_\theta/(k_p.L_{\text{eff}}^2)$ and $B_1 = B_\theta/(k_p.L_{\text{eff}}^2)$.

## 4. Problem Formulation

*4.1. Generality*

*Definition* 1: The LuGre friction model is said to satisfy the energetic passivity condition if there exists a finite constant $b \in R$ such that for $t \geq 0$,

$$\int_0^t s_L(\dot{q}_2(\tau))d\tau = \int_0^t [F_H(\tau)\dot{q}_2(\tau)]d\tau \geq -b^2, \quad (9)$$

https://doi.org/10.1017/S0263574709990336 Published online by Cambridge University Press

where $s_L$ is the energy generated by $F_H$.

*Theorem* 1: Inequality (9) is satisfied if and only if inequality (10) is fulfilled[29]:

$$\frac{1}{F_C} \leq \frac{1}{F_S}\left(1+\frac{\sigma_2}{\sigma_1}\right). \tag{10}$$

*Definition* 2: The teleoperator is said to satisfy the energetic passivity condition if there exists a finite constant $d \in R$ such that for every $F_1$, $F_2$, and for $t \geq 0$,

$$\int_0^t s_{1/k_f}(\dot{Q}_1(\tau), \dot{q}_2(\tau), F_1(\tau), F_2(\tau))\mathrm{d}\tau = \int_0^t \left[\frac{1}{k_f}F_1(\tau)\frac{\dot{Q}_1(\tau)}{k_p} + F_2(\tau)\dot{q}_2(\tau)\right]\mathrm{d}\tau \geq -d^2, \tag{11}$$

where $s_{1/k_f}$ is the scaled net energy transferred between environment and teleoperator.

*Definition* 3: The controller is said to satisfy the energetic passivity condition if there exists a finite constant $c \in R$ such that for $t \geq 0$,

$$\int_0^t s_c(\dot{Q}_1(\tau), \dot{q}_2(\tau), T_1(\tau), T_2(\tau))\mathrm{d}\tau = \int_0^t \left[\frac{1}{k_f}T_1(\tau)\frac{\dot{Q}_1(\tau)}{k_p} + T_2(\tau)\dot{q}_2(\tau)\right]\mathrm{d}\tau \leq c^2, \tag{12}$$

where $s_c$ is the scaled energy generated by the controllers $T_1$ and $T_2$.

*Theorem* 2: Passivity of the controller (Definition 3) results in passivity of the teleoperator (Definition 2).

*Proof*: Scaled kinetic energy of the teleoperation system and its derivative can be defined as follows:

$$\begin{aligned} k_{1/k_f}(t) &= \frac{1}{k_f}\frac{1}{2}J_\theta\dot{\theta}^2(t) + \frac{1}{2}M_2\dot{q}_2(t)^2 \\ \frac{\mathrm{d}}{\mathrm{d}t}k_{1/k_f}(t) &= \frac{1}{k_f k_p}[T_1+F_1]\dot{Q}_1 + [T_2+F_2]\dot{q}_2 \\ &\quad - \frac{1}{k_f k_p}B_1\dot{Q}_1^2 - B_2\dot{q}_2^2 - K_2 q_2\dot{q}_2 - F_H\dot{q}_2 \end{aligned} \tag{13}$$

By integrating from both sides of Eq. (13), supposing passivity of the controller (Definition 3), and knowing that $k_{1/k_f}(t) = 0$, it is concluded that

$$\begin{aligned} &\int_0^t \left[\frac{1}{k_f k_p}F_1(\tau)\dot{Q}_1(\tau) + F_2(\tau)\dot{q}_2(\tau)\right]\mathrm{d}\tau \\ &\geq -k_{1/k_f}(0) - c^2 + \underbrace{\int_0^t \left[\frac{1}{k_f k_p}B_1\dot{Q}_1^2 + B_2\dot{q}_2^2\right]\mathrm{d}\tau}_{1:\geq 0} \\ &\quad + \underbrace{\int_0^t K_2 q_2(\tau)\dot{q}_2(\tau)\mathrm{d}\tau}_{2:\geq 0} + \underbrace{\int_0^t [F_H\dot{q}_2(\tau)\mathrm{d}\tau}_{3:\geq -b^2} \\ &\geq -k_{1/k_f}(0) - c^2 - b^2 = -d^2. \therefore \end{aligned} \tag{14}$$

In Eq. (14), part 1 is obviously positive. Part 2 is positive as well based on the integration-by-part concept. Part 3 is greater than $-b^2$, according to Theorem 1 for the identified parameters of Table III.

Theorem 2 enables us to check the passivity of the controller instead of checking the passivity of the teleoperator in order to judge the passivity of the whole system, which is more inconvenient.

### 4.2. Control objectives

The control framework should be designed such that the following objectives are fulfilled: (1) the closed-loop teleoperator remains robustly stable (passive), i.e. even in the presence of dynamic parameter uncertainty; (2) position signals of the master and slave robots track each other not only in free space motion, but also during contact, that is, $\forall(F_1, F_2)$, $q_E = Q_1 - q_2 \to 0$; (3) the forces exerted on the two robots satisfactorily track each other. Equations (2) and (3) altogether imply transparency.[13]

When position tracking occurs, the dynamic representation of the whole system would be as follows:

$$M_L\ddot{q}_L(t) + B_L\dot{q}_L(t) + K_L(t) = T_L + F_L, \tag{15}$$

where $\dot{q}_L(t) = \dot{Q}_1(t) = \dot{q}_2(t)$. Also,

$$\begin{aligned} M_L &= \frac{M_1}{k_f} + M_2, \quad B_L = \frac{B_1}{k_f} + B_2, \\ K_L(t) &= F_H(t) + K_2 q_L(t), \quad F_L = \frac{F_1}{k_f} + F_2, \\ T_L &= \frac{T_1}{k_f} + T_2. \end{aligned} \tag{16}$$

The letter "L" stands for the locked system.

## 5. Decomposition of the 2-DOF Teleoperator

Using a transformation matrix, $S$, the 2-DOF master–slave is decomposed into two robot-like 1-DOF systems: the *shape* and the *locked*. This transformation matrix must satisfy the following objectives: (1) the teleoperator kinetic energy can be written as the summation of the shape and locked system kinetic energies; that means, $S$ should be diagonal. (2) Inertia of the locked system should be what it is expected to be, i.e. $M_L = M_1/k_f + M_2$. The following fulfills these objectives:

$$\begin{bmatrix} V_L \\ q_E \end{bmatrix} = \underbrace{\begin{bmatrix} x & y \\ 1 & -1 \end{bmatrix}}_{=:S}\begin{bmatrix} \dot{Q}_1 \\ \dot{q}_2 \end{bmatrix} z, \tag{17}$$

where

$$x = \frac{M_1/k_f}{M_1/k_f + M_2}, \quad y = \frac{M_2}{M_1/k_f + M_2}. \tag{18}$$

Arranging Eqs. (4) and (5) in a matrix form, putting Eq. (17) into them, and then multiplying both sides by $S^{-T}$ would

https://doi.org/10.1017/S0263574709990336 Published online by Cambridge University Press

result in the following:

$$\begin{aligned}&\text{(i)}\ \underbrace{M_{\mathrm{E}}\ddot{q}_{\mathrm{E}}(t)+B_{\mathrm{E}}\dot{q}_{\mathrm{E}}(t)}_{\substack{\text{Shaped}\ \text{system}\ \text{dynamics}}}+\underbrace{B_{\mathrm{EL}}\dot{q}_{\mathrm{L}}(t)}_{\text{Coupling}}+K_{\mathrm{E}}(t)=T_{\mathrm{E}}+F_{\mathrm{E}}\\&\text{(ii)}\ \underbrace{M_{\mathrm{L}}\ddot{q}_{\mathrm{L}}(t)+B_{\mathrm{L}}\dot{q}_{\mathrm{L}}(t)}_{\substack{\text{Locked}\ \text{system}\ \text{dynamics}}}+\underbrace{B_{\mathrm{LE}}\dot{q}_{\mathrm{E}}(t)}_{\text{Coupling}}+K_{\mathrm{L}}(t)=T_{\mathrm{L}}+F_{\mathrm{L}}\end{aligned}\text{'} \tag{19}$$

where

$$B_{\mathrm{LE}}=\frac{B_1M_2-M_1B_2}{M_1+k_{\mathrm{f}}M_2},\quad B_{\mathrm{EL}}=B_{\mathrm{LE}},\quad B_{\mathrm{E}}=\frac{B_1B_2}{B_1+k_{\mathrm{f}}B_2},$$
$$M_{\mathrm{E}}=\frac{M_1M_2}{M_1+k_{\mathrm{f}}M_2},\quad K_{\mathrm{E}}=-\frac{M_1}{M_1+M_2k_{\mathrm{f}}}K_{\mathrm{L}},$$
$$T_{\mathrm{E}}=\frac{[T_1M_2-M_1T_2]}{M_1+k_{\mathrm{f}}M_2},\quad F_{\mathrm{E}}=\frac{[F_1M_2-M_1F_2]}{M_1+k_{\mathrm{f}}M_2}$$

$q_{\mathrm{E}}$ is the position tracking error, $q_{\mathrm{L}}$ represents the position of the locked system, $F_{\mathrm{L}}$ and $F_{\mathrm{E}}$ represent the force exerting on the shape and locked systems, respectively. $B_{\mathrm{EL}}$ and $B_{\mathrm{LE}}$ correlate the two equations in Eq. (19). Unlike in ref. [15], the two following essential characteristics *are not* satisfied for the current system (19):

$$\begin{aligned}&(1)\ \dot{M}_{\mathrm{L}}-2B_{\mathrm{L}}\text{ and }\dot{M}_{\mathrm{E}}-2B_{\mathrm{E}}\text{ are skew-symmetric,}\\&(2)\ B_{\mathrm{LE}}+B_{\mathrm{EL}}=0.\end{aligned} \tag{20}$$

Since Eq. (20) is not fulfilled for the decomposition of the teleoperator used in this research, all theorems, lemmas, and propositions provided in ref. [15] are inapplicable and must be reestablished for hysteresis-type nonlinear systems.

## 6. Control Design

### *6.1. Position tracking controller*

This controller is applied to the shape system and aims to guarantee tracking of the master and slave position signals (i.e. $q_{\mathrm{E}}=Q_1-q_2\to 0$) not only in free space motion, but also during contact (i.e. for any $F_1$, $F_2$). To reach this goal, the following modified PD controller is proposed:

$$T_{\mathrm{E}}=-K_{\mathrm{v}}\dot{q}_{\mathrm{E}}-K_{\mathrm{p}}q_{\mathrm{E}}-\hat{F}_{\mathrm{E}}(t)+B_{\mathrm{EL}}\dot{q}_{\mathrm{L}}+B_{\mathrm{E}}\dot{q}_{\mathrm{E}}+\hat{K}_{\mathrm{E}}. \tag{21}$$

Here $K_{\mathrm{v}}$ and $K_{\mathrm{p}}$ are derivative and proportional gains, respectively, and $\hat{F}_{\mathrm{E}}(t)$ is added to guarantee position tracking not only in free space motion, but also during contact. The hat sign above $F_{\mathrm{E}}$ and $K_{\mathrm{E}}$ refers to force measurement inaccuracy and dynamic parameter uncertainty, respectively.

*Theorem* 3: Suppose $F_1$, $F_2$, $\dot{Q}_1$, and $\dot{q}_2$ are bounded. If dynamic parameters of the master and slave robots and measured force signals are true values, then the shape system will asymptotically converge to the equilibrium point $(q_{\mathrm{E}},\dot{q}_{\mathrm{E}})=(0,0)$. Otherwise, if there is any dynamic parameter uncertainty and/or force measurement inaccuracy, then $(q_{\mathrm{E}},\dot{q}_{\mathrm{E}})$ will ultimately converge to a bounded value.

*Proof*: Substituting Eq. (21) into (19(i)) will result in

$$M_{\mathrm{E}}\ddot{q}_{\mathrm{E}}+K_{\mathrm{v}}\dot{q}_{\mathrm{E}}+K_{\mathrm{p}}q_{\mathrm{E}}=\underbrace{(F_{\mathrm{E}}-\hat{F}_{\mathrm{E}})}_{\tilde{F}_{\mathrm{E}}}+\underbrace{(K_{\mathrm{E}}-\hat{K}_{\mathrm{E}})}_{\tilde{K}_{\mathrm{E}}}=\tilde{F}(t). \tag{22}$$

Now, the following candidate Lyapunov function is proposed:

$$V(t)=\frac{1}{2}M_{\mathrm{E}}\dot{q}_{\mathrm{E}}^2+\frac{1}{2}K_{\mathrm{p}}q_{\mathrm{E}}^2+\varepsilon\, q_{\mathrm{E}}M_{\mathrm{E}}\dot{q}_{\mathrm{E}}, \tag{23}$$

where $\varepsilon>0$ is a sufficiently small scalar such that $V(t)$ remains positive-definite. The last term in Eq. (23) guarantees asymptotic convergence to the equilibrium point.

$$\frac{\mathrm{d}}{\mathrm{d}t}V(t)=-\left[(K_{\mathrm{v}}-\varepsilon\, M_{\mathrm{E}})\dot{q}_{\mathrm{E}}^2+\varepsilon\, K_{\mathrm{p}}q_{\mathrm{E}}^2+\varepsilon\, q_{\mathrm{E}}K_{\mathrm{v}}\dot{q}_{\mathrm{E}}\right]$$
$$+(\dot{q}_{\mathrm{E}}+\varepsilon\, q_{\mathrm{E}})\tilde{\tilde{F}}(t). \tag{24}$$

According to Eq. (24), there is always a sufficiently small $\varepsilon$ such that

$$\frac{\mathrm{d}}{\mathrm{d}t}V(t)\le-\gamma V(t)+(\dot{q}_{\mathrm{E}}+\varepsilon\, q_{\mathrm{E}})\tilde{\tilde{F}}(t). \tag{25}$$

Here $\gamma>0$ is the rate of convergence to the equilibrium point. As $F_1$, $F_2$, $\dot{Q}_1$, and $\dot{q}_2$ are supposed to be bounded,[15] $\tilde{\tilde{F}}(t)$ is bounded as well. Thus, for some $\lambda>0$,

$$\frac{\mathrm{d}}{\mathrm{d}t}V(t)\le-\gamma.V(t)+\lambda V^{\frac{1}{2}}(t)\tilde{\tilde{F}}_{\max}, \tag{26}$$

where $\tilde{\tilde{F}}_{\max}\ge|\tilde{\tilde{F}}(t)|$ for $t\ge 0$.

According to Eq. (26), if $\tilde{\tilde{F}}(t)=0$, then $(q_{\mathrm{E}},\dot{q}_{\mathrm{E}})$ will exponentially converge to the equilibrium point (0,0). Otherwise, if $\tilde{\tilde{F}}(t)\neq 0$ but bounded, $(q_{\mathrm{E}},\dot{q}_{\mathrm{E}})$ will ultimately converge to the following value:

$$\bar{V}=\left[\frac{\lambda}{\gamma}\tilde{\tilde{F}}_{\max}\right]^2. \tag{27}$$

*Proposition* 1: Inequality (26) is not satisfied unless $K_{\mathrm{v}}>(\varepsilon+\frac{\gamma}{2})M_{\mathrm{E}}$ and $\varepsilon>\frac{\gamma}{2}$.

*Proof*: The proof of this proposition is omitted for brevity.[28]

### *6.2. Force tracking controller*

To gain tracking of the scaled force signals exerted on the master and slave robots as a measure of transparency, an impedance controller is employed. This controller induces the following desired dynamics to the locked system dynamics (19(ii)):

$$M'_{\mathrm{L}}\ddot{q}_{\mathrm{L}}(t)+B'_{\mathrm{L}}\dot{q}_{\mathrm{L}}(t)+K'_{\mathrm{L}}q_{\mathrm{L}}(t)=F_{\mathrm{L}}. \tag{28}$$

$M'_{\mathrm{L}}$, $B'_{\mathrm{L}}$, and $K'_{\mathrm{L}}$ are the desired inertia, viscous damping, and stiffness of the closed-loop locked system. From Eq. (16), $F_{\mathrm{L}}$ is the force tracking error. Thus, to achieve ideal force tracking (when $F_{\mathrm{L}}$ is set to zero), $M'_{\mathrm{L}}$, $B'_{\mathrm{L}}$, and $K'_{\mathrm{L}}$ have to be set to zero. But, it is not feasible as the closed-loop locked system will disappear. Hence, $K'_{\mathrm{L}}$ is set to zero

https://doi.org/10.1017/S0263574709990336 Published online by Cambridge University Press

and $M'_{\mathrm{L}}$ and $B'_{\mathrm{L}}$ are selected as small, as transient response considerations of the closed-loop system are satisfactory.

Substituting $\ddot{q}_{\mathrm{L}}$ from Eq. (28) into (19(ii)), the locked system controller is determined:

$$T_{\mathrm{L}} = \left(\frac{M_{\mathrm{L}}}{M'_{\mathrm{L}}} - 1\right) F_{\mathrm{L}} + \left(B_{\mathrm{L}} - B'_{\mathrm{L}}\frac{M_{\mathrm{L}}}{M'_{\mathrm{L}}}\right)\dot{q}_{\mathrm{L}} + \left(K_{\mathrm{L}} - K'_{\mathrm{L}}\frac{M_{\mathrm{L}}}{M'_{\mathrm{L}}}q_{\mathrm{L}}\right) + B_{\mathrm{LE}}\dot{q}_{\mathrm{E}} \tag{29}$$

## 7. Stability Analysis

### *7.1. Keeping controllers passive*

It is well known that the whole teleoperation system will be passive if the teleoperator remains passive. It is based on the technical assumption that the human operator and the environment are assumed to be passive.[30] Also, according to Theorem 2, the passivity of the controller results in the passivity of the teleoperator. Hence, to make the whole system passive, it is enough to keep the controllers passive. Controllers of the shape and locked systems, Eqs. (21) and (29), can be rearranged in a matrix form:

$$\begin{bmatrix} T_{\mathrm{L}} \\ T_{\mathrm{E}} \end{bmatrix} = \begin{bmatrix} B_{\mathrm{L}} - B'_{\mathrm{L}}\frac{M_{\mathrm{L}}}{M'_{\mathrm{L}}} & B_{\mathrm{LE}} \\ B_{\mathrm{EL}} & B_{\mathrm{E}} - K_{\mathrm{v}} \end{bmatrix} \begin{bmatrix} \dot{q}_{\mathrm{L}} \\ \dot{q}_{\mathrm{E}} \end{bmatrix} + \begin{bmatrix} -K'_{\mathrm{L}}\frac{M_{\mathrm{L}}}{M'_{\mathrm{L}}} \\ -K_{\mathrm{p}} \end{bmatrix} \begin{bmatrix} q_{\mathrm{L}} \\ q_{\mathrm{E}} \end{bmatrix} + \begin{bmatrix} \left(\frac{M_{\mathrm{L}}}{M'_{\mathrm{L}}} - 1\right) F_{\mathrm{L}} + K_{\mathrm{L}} \\ -\hat{F}_{\mathrm{E}} + \hat{K}_{\mathrm{E}} \end{bmatrix}. \tag{30}$$

To detect troublesome terms within controller matrix (30), two sides of this matrix equation are multiplied by $[V_{\mathrm{L}} \quad \dot{q}_{\mathrm{E}}]$, where $V_{\mathrm{L}} = \dot{q}_{\mathrm{L}}$:

$$\begin{aligned} T_{\mathrm{L}}V_{\mathrm{L}} + T_{\mathrm{E}}\dot{q}_{\mathrm{E}} &= \underbrace{B_{\mathrm{L}}V_{\mathrm{L}}^2 + B_{\mathrm{E}}\dot{q}_{\mathrm{E}}^2 + 2B_{\mathrm{LE}}V_{\mathrm{L}}\dot{q}_{\mathrm{E}}}_{=:\mathrm{I}} \\ &\quad \underbrace{- B'_{\mathrm{L}}\frac{M_{\mathrm{L}}}{M'_{\mathrm{L}}}V_{\mathrm{L}}^2 - K_{\mathrm{v}}\dot{q}_{\mathrm{E}}^2}_{=:\mathrm{II}} \underbrace{- K'_{\mathrm{L}}\frac{M_{\mathrm{L}}}{M'_{\mathrm{L}}}q_{\mathrm{L}}V_{\mathrm{L}} - K_{\mathrm{p}}q_{\mathrm{E}}\dot{q}_{\mathrm{E}}}_{=:\mathrm{III}} \\ &\quad + \underbrace{\left[\left(\frac{M_{\mathrm{L}}}{M'_{\mathrm{L}}} - 1\right)F_{\mathrm{L}} + K_{\mathrm{L}}\right]V_{\mathrm{L}}}_{=:\mathrm{IV}} + \underbrace{\dot{q}_{\mathrm{E}}[-\hat{F}_{\mathrm{E}} + \hat{K}_{\mathrm{E}}]}_{=:\mathrm{V}}. \end{aligned} \tag{31}$$

Part I in Eq. (31) is an absolutely active term, since it is equal to $\frac{B_1}{k_{\mathrm{f}}}\dot{Q}_1^2 + B_2\dot{q}_2^2$, which is always positive (see Eq. (12)). Part II is absolutely passive, since it is always negative. Part III is also passive based on the integration-by-part concept. Parts IV and V are potentially active terms depending on the sign of the velocity signals.

Now, to keep the controller (30) passive, troublesome terms (i.e. the terms generating parts I, IV, and V) should remain bounded. Hence, the energy generated by these troublesome terms is taken from some virtual flywheels with bounded kinetic energy deposited on them. Four 1-DOF virtual flywheels (all constructed in software) are designed: ${}^{L_i}M_{\mathrm{f}}{}^{L_i}\ddot{x}_{\mathrm{f}} = {}^{L_i}T_{\mathrm{f}}$ (the locked system flywheels) and ${}^{E_i}M_{\mathrm{f}}{}^{E_i}\ddot{x}_{\mathrm{f}} = {}^{E_i}T_{\mathrm{f}}$ (the shape system flywheels) ($i \in \{1, 2\}$); ${}^{*}M_{\mathrm{f}}$, ${}^{*}x_{\mathrm{f}}$, and ${}^{*}T_{\mathrm{f}}$ are the inertia, position, and torque exerted on the flywheels ($* \in \{L_i, E_i\}$). The following NSD arrangement of controller (30) using the virtual flywheel concept will guarantee passivity of the controller:

$$\begin{bmatrix} T_{\mathrm{L}} \\ T_{\mathrm{E}} \\ {}^{L_1}T_{\mathrm{f}} \\ {}^{L_2}T_{\mathrm{f}} \\ {}^{E_1}T_{\mathrm{f}} \\ {}^{E_2}T_{\mathrm{f}} \end{bmatrix} = \underbrace{\begin{bmatrix} -\Gamma_d(t) & 0 & \Pi_\varphi^1(t) & \Pi_\varphi^2(t) & 0 & 0 \\ 0 & \Delta_d(t) & 0 & 0 & \Sigma_{\mathrm{E}}^1(t) & \Sigma_{\mathrm{E}}^2(t) \\ -\Pi_\varphi^1(t) & 0 & 0 & 0 & 0 & 0 \\ -\Pi_\varphi^2(t) & 0 & 0 & 0 & 0 & 0 \\ 0 & -\Sigma_{\mathrm{E}}^1(t) & 0 & 0 & 0 & 0 \\ 0 & -\Sigma_{\mathrm{E}}^2(t) & 0 & 0 & 0 & 0 \end{bmatrix}}_{\Omega(t)} \times \begin{bmatrix} V_{\mathrm{L}} \\ \dot{q}_{\mathrm{E}} \\ {}^{L_1}\dot{x}_{\mathrm{f}} \\ {}^{L_2}\dot{x}_{\mathrm{f}} \\ {}^{E_1}\dot{x}_{\mathrm{f}} \\ {}^{E_2}\dot{x}_{\mathrm{f}} \end{bmatrix} + \begin{bmatrix} -K'_{\mathrm{L}}\frac{M_{\mathrm{L}}}{M'_{\mathrm{L}}}q_{\mathrm{L}} \\ -K_{\mathrm{p}}q_{\mathrm{E}} \\ 0 \\ 0 \\ 0 \\ 0 \end{bmatrix}. \tag{32}$$

$\Omega(t)$ is an NSD matrix. In Eq. (32), $(\Pi_\varphi^1(t), \Pi_\varphi^2(t))$ and $(\Sigma_\varphi^1(t), \Sigma_\varphi^2(t))$ are designed such that they generate $((\frac{M_{\mathrm{L}}}{M'_{\mathrm{L}}} - 1)F_{\mathrm{L}}, \{K_{\mathrm{L}} + B_{\mathrm{L}}\dot{q}_{\mathrm{L}} + B_{\mathrm{LE}}\dot{q}_{\mathrm{E}}\})$ and $(-\hat{F}_{\mathrm{E}}, \{\hat{K}_{\mathrm{E}} + B_{\mathrm{EL}}\dot{q}_{\mathrm{L}} + B_{\mathrm{E}}\dot{q}_{\mathrm{E}}\})$, respectively. Now, if ${}^{L_i}\dot{x}_{\mathrm{f}}\Pi_\varphi^i(t)V_{\mathrm{L}} = -\frac{\mathrm{d}}{\mathrm{d}t}(\frac{1}{2}{}^{L_i}M_{\mathrm{L}}{}^{L_i}\dot{x}_{\mathrm{f}}^2)$ and ${}^{E_i}\dot{x}_{\mathrm{f}}\Sigma_{\mathrm{E}}^i(t)\dot{q}_{\mathrm{E}} = -\frac{\mathrm{d}}{\mathrm{d}t}(\frac{1}{2}{}^{E_i}M_{\mathrm{f}}{}^{E_i}\dot{x}_{\mathrm{f}}^2)$ are satisfied, the required energy to generate $\Pi_\varphi^i$ and $\Sigma_{\mathrm{E}}^i$ would be taken from the locked and shape system flywheels, respectively.

To prove intrinsic passivity of the NSD structure (32), both sides of Eq. (32) are multiplied by $[V_{\mathrm{L}} \quad \dot{q}_{\mathrm{E}} \quad {}^{L_1}\dot{x}_{\mathrm{f}} \quad {}^{L_2}\dot{x}_{\mathrm{f}} \quad {}^{E_1}\dot{x}_{\mathrm{f}} \quad {}^{E_2}\dot{x}_{\mathrm{f}}]$. From (32), we have

$$T_{\mathrm{L}}V_{\mathrm{L}} + T_{\mathrm{E}}V_{\mathrm{E}} + {}^{L_1}T_{\mathrm{f}}{}^{L_1}\dot{x}_{\mathrm{f}} + {}^{L_2}T_{\mathrm{f}}{}^{L_2}\dot{x}_{\mathrm{f}} + {}^{E_1}T_{\mathrm{f}}{}^{E_1}\dot{x}_{\mathrm{f}} + {}^{E_2}T_{\mathrm{f}}{}^{E_2}\dot{x}_{\mathrm{f}} \le \begin{bmatrix} V_{\mathrm{L}} & \dot{q}_{\mathrm{E}} \end{bmatrix} \begin{bmatrix} -K'_{\mathrm{L}}\frac{M_{\mathrm{L}}}{M'_{\mathrm{L}}}q_{\mathrm{L}} \\ -K_{\mathrm{p}}q_{\mathrm{E}} \end{bmatrix}. \tag{33}$$

From Eq. (33) and $s_{\mathrm{c}}(\dot{Q}_1, \dot{q}_2, T_1, T_2) = T_{\mathrm{L}}V_{\mathrm{L}} + T_{\mathrm{E}}\dot{q}_{\mathrm{E}}$,[28] it can be concluded that

$$\begin{aligned} \int_0^t s_{\mathrm{c}}(\tau)\mathrm{d}\tau &= \int_0^t (T_{\mathrm{L}}V_{\mathrm{L}} + T_{\mathrm{E}}\dot{q}_{\mathrm{E}})\mathrm{d}\tau \\ &= \underbrace{-K'_{\mathrm{L}}\frac{M_{\mathrm{L}}}{M'_{\mathrm{L}}}q_{\mathrm{L}}V_{\mathrm{L}} - K_{\mathrm{p}}q_{\mathrm{E}}\dot{q}_{\mathrm{E}}}_{=:I} \\ &\quad - \int_0^t \sum_{i=1}^{2} \left({}^{L_i}T_{\mathrm{f}}{}^{L_i}\dot{x}_{\mathrm{f}} + {}^{E_i}T_{\mathrm{f}}{}^{E_i}\dot{x}_{\mathrm{f}}\right)\mathrm{d}\tau \\ &\le \sum_{i=1}^{2}\left(\frac{1}{2}{}^{L_i}M_{\mathrm{f}}{}^{L_i}\dot{x}_{\mathrm{f}}^2(t) + \frac{1}{2}{}^{E_i}M_{\mathrm{f}}{}^{E_i}\dot{x}_{\mathrm{f}}^2(t)\right) \end{aligned},$$

https://doi.org/10.1017/S0263574709990336 Published online by Cambridge University Press

$$+\sum_{i=1}^{2}\left(\frac{1}{2}{}^{L_i}M_{\mathrm{f}}{}^{L_i}\dot{x}_{\mathrm{f}}^2(0)+\frac{1}{2}{}^{E_i}M_{\mathrm{f}}{}^{E_i}\dot{x}_{\mathrm{f}}^2(0)\right)$$
$$\leq\sum_{i=1}^{2}\left(\frac{1}{2}{}^{L_i}M_{\mathrm{f}}{}^{L_i}\dot{x}_{\mathrm{f}}^2(0)+\frac{1}{2}{}^{E_i}M_{\mathrm{f}}{}^{E_i}\dot{x}_{\mathrm{f}}^2(0)\right)\quad,$$
$$=c^2\Rightarrow\int_0^t s_{\mathrm{c}}(\tau)\mathrm{d}\tau\leq c^2\quad\therefore$$

which means NSD structure (32) fulfills controller passivity condition (12). It should be noticed that part I above is negative due to the integration-by-part concept.

### *7.2. Finding parameters of the NSD structure*

The entries $\Pi_{\varphi}^{i}$, $\Sigma_{\mathrm{E}}^{i}$, $\Gamma_d(t)$, and $\Delta_d(t)$ in (32) should be now designed such that the control architecture (30) is duplicated:

$$\begin{aligned}
&\text{(i) } \Gamma_d(t)=-\left[1-g\left({}^{L_1}\dot{x}_{\mathrm{f}}\right){}^{L_1}\dot{x}_{\mathrm{f}}\right]B_{\mathrm{L}}'\frac{M_{\mathrm{L}}}{M_{\mathrm{L}}'}\\
&\text{(ii) } \Pi_{\varphi}^{1}(t)=\left(\frac{M_{\mathrm{L}}}{M_{\mathrm{L}}'}-1\right)F_{\mathrm{L}}\cdot g\left({}^{L_1}\dot{x}_{\mathrm{f}}\right)\underbrace{-B_{\mathrm{L}}'\frac{M_{\mathrm{L}}}{M_{\mathrm{L}}'}V_{\mathrm{L}}\cdot g\left({}^{L_1}\dot{x}_{\mathrm{f}}\right)}_{\text{Energy recapture}}\\
&\text{(iii) } \Pi_{\varphi}^{2}(t)=\left(K_{\mathrm{L}}+B_{\mathrm{L}}V_{\mathrm{L}}+B_{\mathrm{LE}}\dot{q}_{\mathrm{E}}\right)\cdot g\left({}^{L_2}\dot{x}_{\mathrm{f}}\right)\\
&\text{(iv) } \Delta_d(t)=-\left[1-g\left({}^{E_1}\dot{x}_{\mathrm{f}}\right){}^{E_1}\dot{x}_{\mathrm{f}}\right]K_{\mathrm{v}}\\
&\text{(v) } \Sigma_{\mathrm{E}}^{1}(t)=\underbrace{-g\left({}^{E_1}\dot{x}_{\mathrm{f}}\right)K_{\mathrm{v}}\dot{q}_{\mathrm{E}}}_{\text{Energy recapture}}+\frac{P_1(t)}{{}^{E_1}\dot{x}_{\mathrm{f}}}(-\hat{F}_{\mathrm{E}})\\
&\text{(vi) } \Sigma_{\mathrm{E}}^{2}(t)=\frac{P_2(t)}{{}^{E_2}\dot{x}_{\mathrm{f}}}(B_{\mathrm{EL}}\dot{q}_{\mathrm{L}}+B_{\mathrm{E}}\dot{q}_{\mathrm{E}}+\hat{K}_{\mathrm{E}})
\end{aligned}\quad,\tag{34}$$

where $g(x)=\{1/x \text{ if } |x|>f_o,\ 1/f_o\mathrm{sgn}(x) \text{ if } 0<|x|\leq f_o, \text{ and } 1/f_o \text{ if } |x|=0\}$, and $f_o>0$ is a small threshold value of the flywheels speeds ($|{}^{L_i}\dot{x}_{\mathrm{f}}|$, $|{}^{E_i}\dot{x}_{\mathrm{f}}|$) such that the terms $\Sigma_{\mathrm{E}}^{i}$, $\Pi_{\varphi}^{i}$ remain bounded. $P_i(t)$ is a binary number which is 1 when $({}^{E_i}\dot{x}_{\mathrm{f}}, q_{\mathrm{E}}, \dot{q}_{\mathrm{E}})\in C_i$. $C_1$ and $C_2$, two switching regions, will be discussed later.

*Theorem* 4: The decomposed mechanical teleoperator (19) under the NSD implementation (32) and (34) is considered.

(4.1) *Locked system flywheels*: Suppose that $V_{\mathrm{L}}$ and $q_{\mathrm{L}}$ are bounded and ${}^{L_1}\dot{x}_{\mathrm{f}}$ and ${}^{L_2}\dot{x}_{\mathrm{f}}$ have been initialized so that

$$\begin{aligned}
&\text{(i) } \frac{1}{2}{}^{L_1}M_{\mathrm{f}}{}^{L_1}\dot{x}_{\mathrm{f}}^2(0)>\frac{1}{2}{}^{L_1}M_{\mathrm{f}}f_o^2+\frac{|\mu|}{1+\mu}\bar{G}_{\mathrm{L}},\\
&\text{(ii) } {}^{L_2}\dot{x}_{\mathrm{f}}(0)>f_o
\end{aligned}\tag{35}$$

where $\bar{G}_{\mathrm{L}}>0$ is the upper bound of $G_{\mathrm{L}}(t)$ satisfying the following inequality:

$$\frac{1}{2}M_{\mathrm{L}}V_{\mathrm{L}}^2(t)+\frac{1}{2}K_{\mathrm{L}}'\frac{M_{\mathrm{L}}}{M_{\mathrm{L}}'}q_{\mathrm{L}}^2(t)<\bar{G}_{\mathrm{L}}\quad\forall t\geq 0.\tag{36}$$

Then, the locked system flywheels will not deplete energy (i.e. $g({}^{L_i}\dot{x}_{\mathrm{f}}){}^{L_i}\dot{x}_{\mathrm{f}}=1$) for all $t\geq 0$ and the locked system flywheels will remain ON.

*Proof*: Suppose that $k_{\mathrm{l}}(t)$ is the augmented locked system energy function such that

$$k_{\mathrm{l}}(t)=\frac{1}{2}M_{\mathrm{L}}V_{\mathrm{L}}^2(t)+\frac{1}{2}K_{\mathrm{L}}'\frac{M_{\mathrm{L}}}{M_{\mathrm{L}}'}q_{\mathrm{L}}^2(t)+\frac{1}{2}{}^{L_1}M_{\mathrm{f}}{}^{L_1}\dot{x}_{\mathrm{f}}^2(t)+\frac{1}{2}{}^{L_2}M_{\mathrm{f}}{}^{L_2}\dot{x}_{\mathrm{f}}^2(t).\tag{37}$$

Then, knowing ${}^{L_i}\dot{x}_{\mathrm{f}}\Pi_{\varphi}^{i}(t)V_{\mathrm{L}}=-\frac{\mathrm{d}}{\mathrm{d}t}(\frac{1}{2}{}^{L_i}M_{\mathrm{L}}{}^{L_i}\dot{x}_{\mathrm{f}}^2)$, it is concluded that

$$\frac{\mathrm{d}}{\mathrm{d}t}k_{\mathrm{l}}(t)=M_{\mathrm{L}}V_{\mathrm{L}}\dot{V}_{\mathrm{L}}+K_{\mathrm{L}}'\frac{M_{\mathrm{L}}}{M_{\mathrm{L}}'}q_{\mathrm{L}}V_{\mathrm{L}}-{}^{L_1}\dot{x}_{\mathrm{f}}\Pi_{\varphi}^{1}(t)V_{\mathrm{L}}-{}^{L_2}\dot{x}_{\mathrm{f}}\Pi_{\varphi}^{2}(t)V_{\mathrm{L}}.\tag{38}$$

Based on the assumption of Theorem 4 (i.e. Eq. (35)), $g({}^{L_i}\dot{x}_{\mathrm{f}}){}^{L_i}\dot{x}_{\mathrm{f}}=1$ at the initial time. Thus, using Eqs. (38), (28), and (34), we have

$$\begin{aligned}
\frac{\mathrm{d}}{\mathrm{d}t}k_{\mathrm{l}}(t)&=\frac{M_{\mathrm{L}}}{M_{\mathrm{L}}'}V_{\mathrm{L}}(F_{\mathrm{L}}-K_{\mathrm{L}}'q_{\mathrm{L}}-B_{\mathrm{L}}'V_{\mathrm{L}})+K_{\mathrm{L}}'\frac{M_{\mathrm{L}}}{M_{\mathrm{L}}'}q_{\mathrm{L}}V_{\mathrm{L}}\\
&\quad-V_{\mathrm{L}}\left[\left(\frac{M_{\mathrm{L}}}{M_{\mathrm{L}}'}-1\right)F_{\mathrm{L}}-B_{\mathrm{L}}'\frac{M_{\mathrm{L}}}{M_{\mathrm{L}}'}V_{\mathrm{L}}\right].\\
&\quad-{}^{L_2}\dot{x}_{\mathrm{f}}\Pi_{\varphi}^{2}(t)V_{\mathrm{L}}=F_{\mathrm{L}}V_{\mathrm{L}}-{}^{L_2}\dot{x}_{\mathrm{f}}\Pi_{\varphi}^{2}(t)V_{\mathrm{L}}
\end{aligned}\tag{39}$$

Substituting $k_{\mathrm{l}}(t)$ in Eq. (39) with Eq. (37) and knowing ${}^{L_2}\dot{x}_{\mathrm{f}}\Pi_{\varphi}^{2}(t)V_{\mathrm{L}}=-\frac{\mathrm{d}}{\mathrm{d}t}(\frac{1}{2}{}^{L_2}M_{\mathrm{L}}{}^{L_2}\dot{x}_{\mathrm{f}}^2)$, it is concluded that

$$\begin{aligned}
&\frac{\mathrm{d}}{\mathrm{d}t}\underbrace{\left(\frac{1}{2}M_{\mathrm{L}}V_{\mathrm{L}}^2(t)+\frac{1}{2}K_{\mathrm{L}}'\frac{M_{\mathrm{L}}}{M_{\mathrm{L}}'}q_{\mathrm{L}}^2(t)\right)}_{G_{\mathrm{L}}(t)}\\
&\quad+\frac{\mathrm{d}}{\mathrm{d}t}\left(\frac{1}{2}{}^{L_1}M_{\mathrm{f}}{}^{L_1}\dot{x}_{\mathrm{f}}^2(t)\right)=F_{\mathrm{L}}V_{\mathrm{L}}\\
&\Rightarrow\frac{\mathrm{d}}{\mathrm{d}t}\left(\frac{1}{2}{}^{L_1}M_{\mathrm{f}}{}^{L_1}\dot{x}_{\mathrm{f}}^2(t)\right)=F_{\mathrm{L}}V_{\mathrm{L}}-\frac{\mathrm{d}}{\mathrm{d}t}G_{\mathrm{L}}(t)\\
&=\frac{1}{\underbrace{\left(\frac{M_{\mathrm{L}}}{M_{\mathrm{L}}'}-1\right)}_{=:\mu}}\left[-\frac{\mathrm{d}}{\mathrm{d}t}\left(\frac{1}{2}{}^{L_1}M_{\mathrm{f}}{}^{L_1}\dot{x}_{\mathrm{f}}^2(t)\right)\right.\\
&\quad\left.+B_{\mathrm{L}}'\tfrac{M_{\mathrm{L}}}{M_{\mathrm{L}}'}V_{\mathrm{L}}^2\right]-\frac{\mathrm{d}}{\mathrm{d}t}G_{\mathrm{L}}(t)\\
&\Rightarrow\frac{\mathrm{d}}{\mathrm{d}t}\left(\frac{1}{2}{}^{L_1}M_{\mathrm{f}}{}^{L_1}\dot{x}_{\mathrm{f}}^2(t)\right)=B_{\mathrm{L}}'V_{\mathrm{L}}^2-\frac{\mu}{\mu+1}\frac{\mathrm{d}}{\mathrm{d}t}G_{\mathrm{L}}(t)\\
&\Rightarrow\frac{\mathrm{d}}{\mathrm{d}t}\left(\frac{1}{2}{}^{L_1}M_{\mathrm{f}}{}^{L_1}\dot{x}_{\mathrm{f}}^2(t)\right)\geq-\frac{\mu}{\mu+1}\frac{\mathrm{d}}{\mathrm{d}t}G_{\mathrm{L}}(t)\\
&\int\\
&\Rightarrow\frac{1}{2}{}^{L_1}M_{\mathrm{f}}{}^{L_1}\dot{x}_{\mathrm{f}}^2(t)-\frac{1}{2}{}^{L_1}M_{\mathrm{f}}{}^{L_1}\dot{x}_{\mathrm{f}}^2(0)\\
&\geq-\frac{\mu}{\mu+1}(G_{\mathrm{L}}(t)-G_{\mathrm{L}}(0))\overset{\mu+1>0}{\geq}\\
&\quad-\frac{|\mu|}{\mu+1}|G_{\mathrm{L}}(t)-G_{\mathrm{L}}(0)|\geq-\frac{|\mu|}{\mu+1}G_{\mathrm{L}}\\
&\Rightarrow\frac{1}{2}{}^{L_1}M_{\mathrm{f}}{}^{L_1}\dot{x}_{\mathrm{f}}^2(t)\geq\frac{1}{2}{}^{L_1}M_{\mathrm{f}}{}^{L_1}\dot{x}_{\mathrm{f}}^2(0)-\frac{|\mu|}{\mu+1}G_{\mathrm{L}}
\end{aligned}$$

https://doi.org/10.1017/S0263574709990336 Published online by Cambridge University Press

Now, according to Eq. (35),

$$\frac{1}{2}{}^{L_1}M_{\rm f}{}^{L_1}\dot{x}_{\rm f}^2(t) \geq \frac{1}{2}{}^{L_1}M_{\rm f}f_o^2 \Leftrightarrow \left|{}^{L_1}\dot{x}_{\rm f}(t)\right| \geq f_o \quad \forall t \geq 0. \tag{40}$$

Based on the proof procedure, part (ii) of Eq. (35) was not engaged and it is just enough that ${}^{L_2}\dot{x}_{\rm f}(0) > f_o$.

(4.2) *Shape system flywheel* 1: The switching region $C_1$ (used to define $P_1(t)$ in Eq. (34)) is defined as the following:

$$C_1 = \left\{ \left({}^{E_1}\dot{x}_{\rm f}, q_{\rm E}, \dot{q}_{\rm E}\right) \middle| \frac{1}{2}{}^{E_1}M_{\rm f}{}^{E_1}\dot{x}_{\rm f}^2(t) > \frac{1}{2}{}^{E_1}M_{\rm f}f_o^2 + \frac{2\hat{F}_{E\max}}{\gamma\delta_{\rm v}}V^{\frac{1}{2}}(t) \right\}, \tag{41}$$

where $\hat{F}_{\max} \geq |\hat{F}(t)| \quad \forall t \geq 0$, $V(t)$ is the Lyapunov function (23), and $\delta_{\rm v} > 0$ is defined such that $V(t) \geq \delta_{\rm v}^2\dot{q}_{\rm E}^2$. Suppose that the shape system flywheel 1 is initialized with an initial velocity so that

$$\frac{1}{2}{}^{E_1}M_{\rm f}{}^{E_1}\dot{x}_{\rm f}^2(0) > \frac{1}{2}{}^{E_1}M_{\rm f}f_o^2 + \frac{2\hat{F}_{E\max}}{\gamma\delta_{\rm v}}V^{\frac{1}{2}}(0), \tag{42}$$

that is, $({}^{E_1}\dot{x}_{\rm f}(0), q_{\rm E}(0), \dot{q}_{\rm E}(0)) \in C_1$. Then, $({}^{E_1}\dot{x}_{\rm f}(t), q_{\rm E}(t), \dot{q}_{\rm E}(t)) \in C_1$ for $t \geq 0$. It means that term $\Pi_{\varphi}^1$ in Eq. (34) remains ON all the time, because $P_1(t) = 1$ for $t \geq 0$. In other words, the shape system 1 never depletes energy below the threshold.

*Proof:* Consider the Lyapunov function (43)[16]

$$V(t) = \frac{1}{2}M_{\rm E}\dot{q}_{\rm E}^2 + \frac{1}{2}K_{\rm p}q_{\rm E}^2 + \varepsilon\, q_{\rm E}M_{\rm E}\dot{q}_{\rm E} \geq \delta_{\rm v}^2\dot{q}_{\rm E}^2. \tag{43}$$

Also, from Eq. (34) and ${}^{E_1}\dot{x}_{\rm f}\Sigma_{\rm E}^1(t)\dot{q}_{\rm E} = -\dfrac{\rm d}{{\rm d}t}\left(\dfrac{1}{2}{}^{E_1}M_{\rm f}{}^{E_1}\dot{x}_{\rm f}^2\right)$, we have

$$\frac{\rm d}{{\rm d}t}\left(\frac{1}{2}{}^{E_1}M_{\rm f}{}^{E_1}\dot{x}_{\rm f}^2(t)\right) = \underbrace{{}^{E_1}\dot{x}_{\rm f}g\left({}^{E_1}\dot{x}_{\rm f}\right)K_{\rm v}\dot{q}_{\rm E}^2}_{\geq 0} + \frac{P_1(t)}{{}^{E_1}\dot{x}_{\rm f}}\hat{F}_{\rm E}\dot{q}_{\rm E}{}^{E_1}\dot{x}_{\rm f} \geq \overbrace{P_1(t)}^{0\text{ or }1}\hat{F}_{\rm E}\dot{q}_{\rm E} \geq -\left|\hat{F}_{\rm E}\right|\left|\dot{q}_{\rm E}\right| \overset{\text{From (43)}}{\geq} -\hat{F}_{E\max}\frac{V(t)^{\frac{1}{2}}}{\delta_{\rm v}} \tag{44}$$

Knowing the fact that $V(t) \leq {\rm e}^{-\gamma t}V(0)$ and integrating from both sides of Eq. (44), it is concluded that

$$\begin{aligned}\frac{1}{2}{}^{E_1}M_{\rm f}{}^{E_1}\dot{x}_{\rm f}^2(t) &\geq \frac{1}{2}{}^{E_1}M_{\rm f}{}^{E_1}\dot{x}_{\rm f}^2(0) - \frac{2\hat{F}_{E\max}}{\gamma\delta_{\rm v}}V(0)^{\frac{1}{2}}\left(1-e^{-\frac{\gamma}{2}t}\right) = \frac{1}{2}{}^{E_1}M_{\rm f}{}^{E_1}\dot{x}_{\rm f}^2(0) \\ &- \frac{2\hat{F}_{E\max}}{\gamma\delta_{\rm v}}V(0)^{\frac{1}{2}} + \frac{2\hat{F}_{E\max}}{\gamma\delta_{\rm v}}(V(0){\rm e}^{-\gamma t})^{\frac{1}{2}} \\ &\geq \frac{1}{2}{}^{E_1}M_{\rm f}{}^{E_1}\dot{x}_{\rm f}^2(0) - \frac{2\hat{F}_{E\max}}{\gamma\delta_{\rm v}}V(0)^{\frac{1}{2}} + \frac{2\hat{F}_{E\max}}{\gamma\delta_{\rm v}}V(t)^{\frac{1}{2}}\end{aligned} \tag{45}$$

Comparing Eqs. (42) and (45), it can be concluded that

$$\frac{1}{2}{}^{E_1}M_{\rm f}{}^{E_1}\dot{x}_{\rm f}^2(t) > \frac{1}{2}{}^{E_1}M_{\rm f}f_o^2 + \frac{2\hat{F}_{E\max}}{\gamma\delta_{\rm v}}V^{\frac{1}{2}}(t). \tag{46}$$

(4.3) *Shape system flywheel* 2: The switching region $C_2$ (used to define $P_2(t)$ in Eq. (34)) is defined as the following:

$$C_2 = \left\{ \left({}^{E_2}\dot{x}_{\rm f}, q_{\rm E}, \dot{q}_{\rm E}\right) \middle| \frac{1}{2}{}^{E_2}M_{\rm f}{}^{E_2}\dot{x}_{\rm f}^2(t) > \frac{1}{2}{}^{E_2}M_{\rm f}f_o^2 + \frac{2A_{\max}}{\gamma\delta_{\rm v}}V^{\frac{1}{2}}(t) \right\}, \tag{47}$$

where $A_{\max} \geq |C_{\rm EL}\dot{q}_{\rm L}(t) + C_{\rm E}\dot{q}_{\rm E}(t) + \hat{K}_{\rm E}|, \quad \forall t \geq 0$. Suppose that the shape system flywheel 2 is initialized with an initial velocity so that

$$\frac{1}{2}{}^{E_2}M_{\rm f}{}^{E_2}\dot{x}_{\rm f}^2(0) > \frac{1}{2}{}^{E_2}M_{\rm f}f_o^2 + \frac{2A_{\max}}{\gamma\delta_{\rm v}}V^{\frac{1}{2}}(0), \tag{48}$$

that is, $({}^{E_2}\dot{x}_{\rm f}(0), q_{\rm E}(0), \dot{q}_{\rm E}(0)) \in C_2$. Then, $({}^{E_2}\dot{x}_{\rm f}(t), q_{\rm E}(t), \dot{q}_{\rm E}(t)) \in C_2$ for all $t \geq 0$.

*Proof*: The procedure is similar to what was presented for shape system flywheel 1. The only difference is replacing $\hat{F}_{E\max}$ with $A_{\max}$.

*Theorem* 5: The decomposed mechanical teleoperator (19) under the NSD implementation (32) and (34) is considered.

(5.1) The closed-loop teleoperator is energetically passive (i.e. satisfies Eq. (11)), even in the presence of inaccurate force sensing $F_1$ and $F_2$ and dynamic parameter uncertainty.

(5.2) The teleoperation system is considered free from inaccuracy of force sensing $F_1$ and $F_2$ and dynamic parameter uncertainty. If $|{}^{E_1}\dot{x}_{\rm f}| \geq f_o$ and Eqs. (42) and (48) are true, then $(q_{\rm E}, \dot{q}_{\rm E}) \to (0, 0)$ exponentially. Also, $\dot{q}_{\rm L}(t) = \dot{Q}_1(t) = \dot{q}_2(t)$. If there is any uncertainty or force measurement inaccuracy, but $|{}^{E_1}\dot{x}_{\rm f}| \geq f_o$ and Eqs. (42) and (48) are true, then $(q_{\rm E}, \dot{q}_{\rm E})$ will converge to a bounded error.

(5.3) The teleoperation system under the assumption of (5.2) is considered. If $|{}^{L_i}\dot{x}_{\rm f}| \geq f_o$ for $t \geq 0$, then the target dynamics (28) and, consequently, force tracking will be achieved.

(5.4) The situation is supposed in which either (even all) of the virtual flywheels is switched off. The closed-loop teleoperator will still remain energetically passive.

*Proof:*

(5.1) The NSD implementation (32) will remain NSD regardless of the presence of inaccurate force sensing $F_1$ and $F_2$ and dynamic parameter uncertainty.

(5.2) Under the presented assumption, it is simply concluded that the NSD implementations (32) and (34) will produce the intended control (30). Then, according to Theorem 3, $(q_{\rm E}, \dot{q}_{\rm E}) \to (0, 0)$ or a bounded error, regarding existence of any uncertainty or inaccuracy.

(5.3) Since $|{}^{L_i}\dot{x}_{\rm f}| \geq f_o$, $g({}^{L_i}\dot{x}_{\rm f}){}^{L_i}\dot{x}_{\rm f} = 1$. Thus, the NSD implementation (32) will duplicate the intended control (30). Therefore, Eq. (28) will be achieved.

(5.4) Even in this situation, the NSD implementation (32) will remain NSD.

https://doi.org/10.1017/S0263574709990336 Published online by Cambridge University Press

Table IV. Designed parameters.

| Symbol | Quantity (SI) | Symbol | Quantity (SI) | Symbol | Quantity (SI) | Symbol | Quantity (SI) |
|---|---|---|---|---|---|---|---|
| $k_p$ | $(10 \times 10^{-5})/(L_{eff}\pi)$ | $M'_L$ | 0.2914 | ${}^{L_2}f_o$ | 4(10) | $\hat{\sigma}_2$ | $2^*\sigma_2$ |
| $k_f$ | 1 | $B'_L$ | $1.51 \times 10^3$ | ${}^{E_1}f_o$ | 2 (30) | $\hat{F}_C$ | $2^*$ $F_C$ |
| $M_1$ | 7.3304 | $K'_L$ | 0 | ${}^{E_2}f_o$ | 1 (35) | $\hat{F}_S$ | $2^*$ $F_s$ |
| $B_1$ | 491.13 | ${}^{E_1}M_f$ | 1.0 | $\tilde{\tilde{F}}_{max}$ | $15 \times 10^2$ | $\hat{v}_{St}$ | $2^*v_{St}$ |
| $M_2$ | 2.17 | ${}^{E_2}M_f$ | 1.0 | $\hat{F}_{E\,max}$ | 4.0 | $K_v$ | 7.45 |
| $B_2$ | 1078.6 | ${}^{L_1}M_f$ | 1.0 | $A_{max}$ | 20 | $K_p$ | $5 \times 10^6$ |
| $K_2$ | $3 \times 10^5$ | ${}^{L_2}M_f$ | 1.0 | $\varepsilon$ | 0.06 | $L_{eff}$ | 0.15 |
| $\hat{M}_1$ | 14.13 | ${}^{L_1}\dot{x}_f(0)$ | 9.0 | $\delta_v$ | 5 | $\hat{L}_{eff}$ | 0.1 |
| $\hat{B}_1$ | $1.44 \times 10^3$ | ${}^{L_2}\dot{x}_f(0)$ | 13.4 | $\bar{G}_L$ | 2 | $\Gamma$ | 0.1 |
| $\hat{M}_2$ | 1.5 | ${}^{E_1}\dot{x}_f(0)$ | 2.4 | $V(0)$ | 0 | $K_g$ | $15 \times 10^2$ |
| $\hat{B}_2$ | 3000 | ${}^{E_2}\dot{x}_f(0)$ | 2.0 | $\hat{\sigma}_0$ | $2^*$ $\sigma_0$ | $\Phi$ | $5 \times 10^{-2}$ |
| $\hat{K}_2$ | $3.2 \times 10^5$ | ${}^{L_1}f_o$ | 3(7) | $\hat{\sigma}_1$ | $2^*$ $\sigma_1$ | | |

## 8. Parameter Design

Position scaling factor $k_p$ is chosen such that for 180° of the master rotation, the slave robot translates its possible 100-$\mu$m displacement. Force scaling factor $k_f$ is designed based on the fact that the slave environment and the slave force sensor (Fig. 2b, No. 4) are one thing in this research. If slave end effecter (Fig. 2b, No. 3) touches the slave force sensor tip and moves it forward around 20 μm, measured force would be around 0.6 N (equivalent stiffness of the environment is $3 \times 10^4$ N/m). That means environmental forces are large enough to be sensed by the operator without any need for magnification. Thus, $k_f$ is set to unity.

In simulation only (Section 9), dynamic parameters within controllers are supposed to be different from the identified parameters in order to simulate uncertainty. In this way, stability and performance of the system in the presence of uncertainty have been investigated before moving to experiment. Other parameters are designed based on either the theoretical discussion in previous sections or at the end of the trial and error in simulation stage. These parameters are shown in Table IV.

## 9. Simulation Results

To verify performance of the designed control architecture, some simulations were organized in MATLAB 7.1/Simulink environment. The system overall block diagram has been shown in Fig. 5.

To demonstrate the performance of the controllers, the following scenario was organized: the human operator is modeled as a spring-damper system with gains of 70 N/m and 50 N · s, respectively.[31] At the 0–3.5 s interval, the master robot is stabilized at the position of 20° without contact with the environment. Then, at the 3.5–12 s interval, the master robot is pushed to a new position, i.e. 60°. While moving the robot to this target, the operator realizes the existence of a hard wall (slave force sensor in this research), receiving ramp-like force feedback (since the environment (= slave force sensor) is a cantilever beam (Fig. 2b, No. 4), behaving like a linear spring). Finally, at 12–15 s, the human operator retracts the master to the origin, again without any contact between the slave and the environment. Figures 6 and 7 show simulation results of this scenario.

In Figs. 6 and 7, the teleoperator is involved with uncertainty (see Table IV). Human/environment forces are

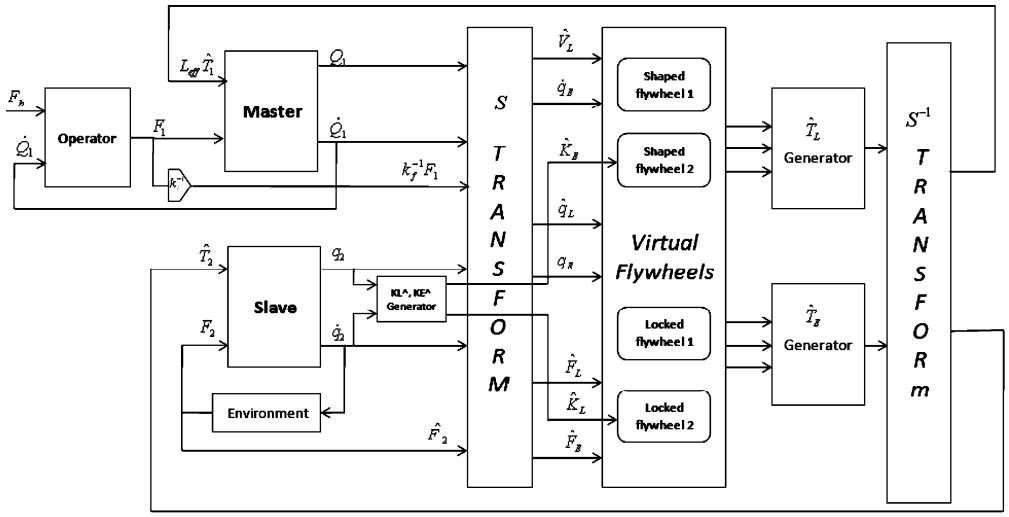


Fig. 5. The system overall block diagram, designed in MATLAB 7.1/Simulink.

https://doi.org/10.1017/S0263574709990336 Published online by Cambridge University Press

Table V. Some parameters should change while moving from simulation to experiment.

| $k_p$ | $M'_L$ | $C'_L$ |
|---|---|---|
| $(10 \times 10^{-5})/(2L_{eff}\pi)$ | 20.0 | 0.01 |

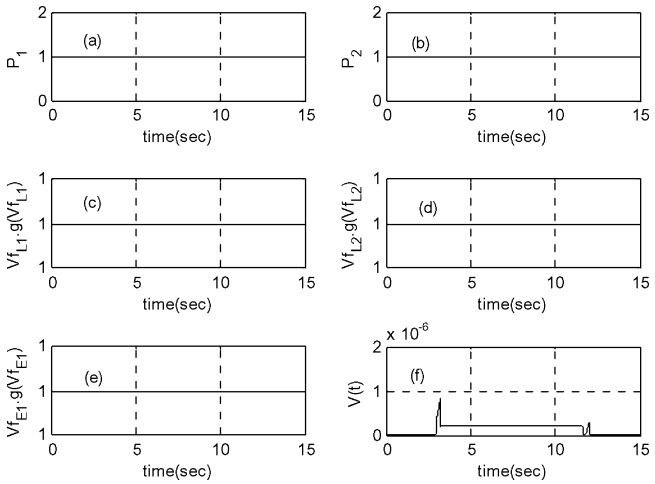


Fig. 6. Simulation results when all flywheels are turned on. Force and position tracking are expected to be satisfactory.

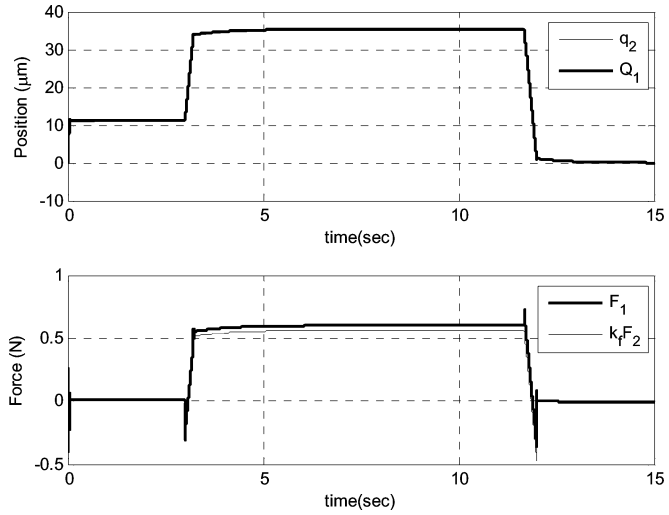


Fig. 7. Simulation results when all flywheels are turned on. Force and position tracking are satisfactory.

assumed to be free of inaccuracy. The following observations are achieved from these two figures:

- According to Fig. 6, all flywheels are turned on. In other words, neither of the flywheels depletes energy below the thresholds. Therefore, according to parts 2 and 3 of Theorem 5, satisfactory position and force tracking are expected. Figure 7 confirms this anticipation.
- The teleoperation system is stable, even in the presence of dynamic parameter uncertainty. This validates robust passivity of the proposed controller, which is stated in part 1 of Theorem 5.
- $V(t)$ decreases to a very small value, due to satisfactory position coordination of the master and slave robots (see Fig. 7). This validates correctness of Theorem 5.

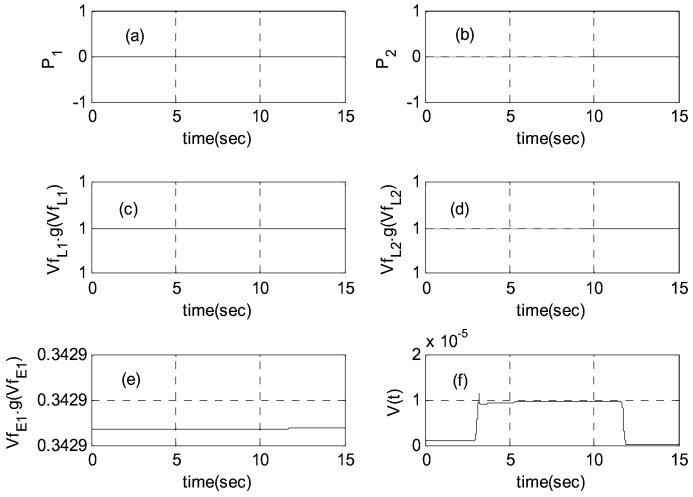


Fig. 8. Shape system flywheels (a), (b), and (e) are off. Position tracking is expected to degrade. $V(t)$ should increase.

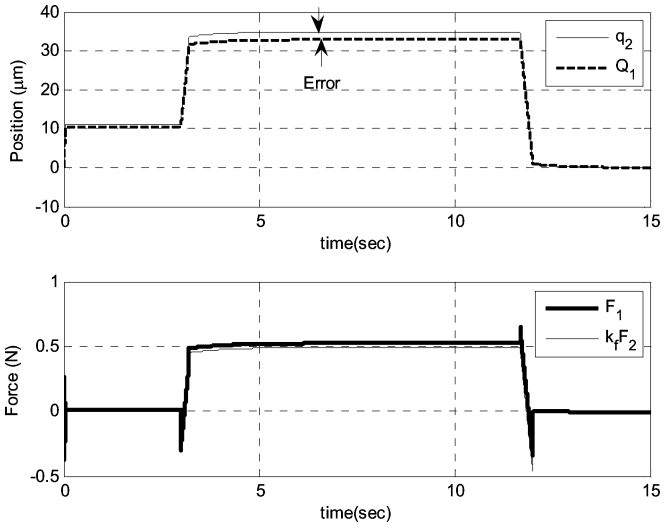


Fig. 9. Shape system flywheels are off. Position tracking is degraded.

- Position tracking is achieved, not only in free space motion ($F_1$, $F_2 = 0$), but also during contact ($F_1$, $F_2 \neq 0$) according to Fig. 7.
- Figure 7 confirms that when the slave robot is pushed against the obstacle (3.5–12 s), the contact force is faithfully reflected to the human.
- During free motion (0–3.5 and 12–15 s), both human and environment forces are expected to be zero. This is confirmed in Fig. 7.

To simulate system performance in the presence of *large* dynamic parameter uncertainty (or force measurement inaccuracy), the direct method is to increase uncertainty. The alternative method is to increase speed threshold of the flywheels, resulting in identical consequences. In this section, the latter approach is utilized.

In the first step (Figs. 8 and 9), only the speed threshold of the shape system flywheels is increased (Table IV, numbers in parentheses) such that the shape system flywheels turn off (Figs. 8a, b, and e). Thus, it is expected that position tracking is sacrificed for stability. This sacrifice

https://doi.org/10.1017/S0263574709990336 Published online by Cambridge University Press

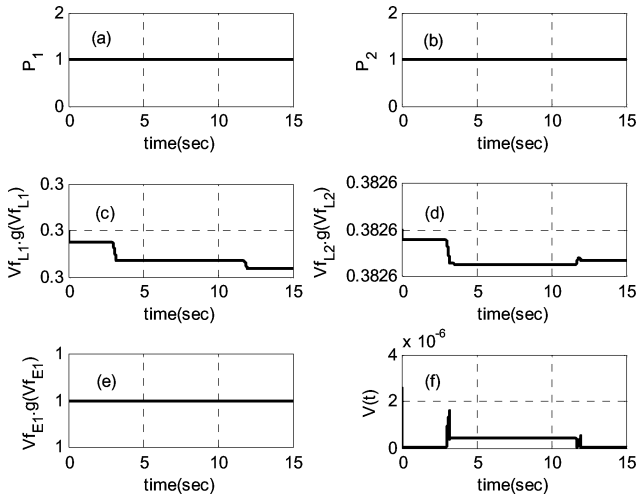


Fig. 10. Locked system flywheels (c) and (d) are depleting energy. Force tracking is expected to degrade.

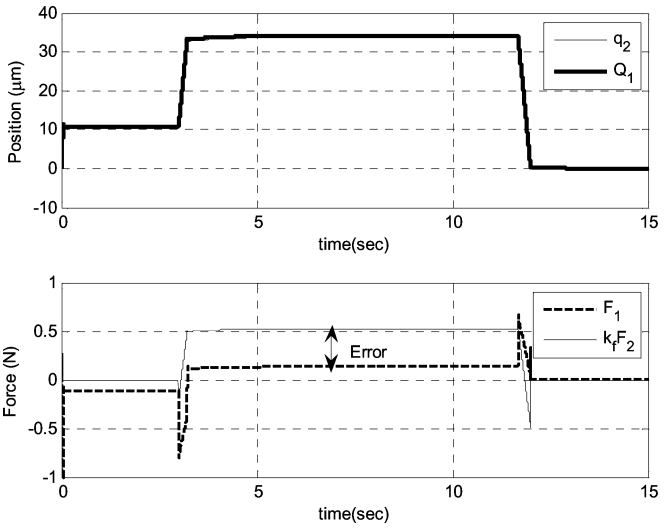


Fig. 11. Locked system flywheels are depleting energy. Force tracking is considerably degraded.

depends on the magnitude of the troublesome terms in $T_E$ which are energetically supported by the shape system flywheels. Figure 9 demonstrates that this dependency is not remarkable.

In the second step (Figs. 10 and 11), only the speed threshold of the locked system flywheels is increased (Table IV, numbers in parentheses) such that the locked system flywheels speeds and, consequently, ${}^{L_1}\dot{x}_f g({}^{L_1}\dot{x}_f) = Vf_{L_1}.g(Vf_{L_1})$ drop below the threshold (Figs. 10 c and d). Thus, it is expected that force tracking be degraded at the cost of stability. The degradation magnitude depends on the magnitude of the troublesome terms in $T_L$ which are energetically supported by the locked system flywheels. Figure 11 shows that this dependency is high.

As human/environment force measurement inaccuracy acts similarly as the model uncertainty (causes flywheels speeds to drop below the thresholds), it will not be simulated here.

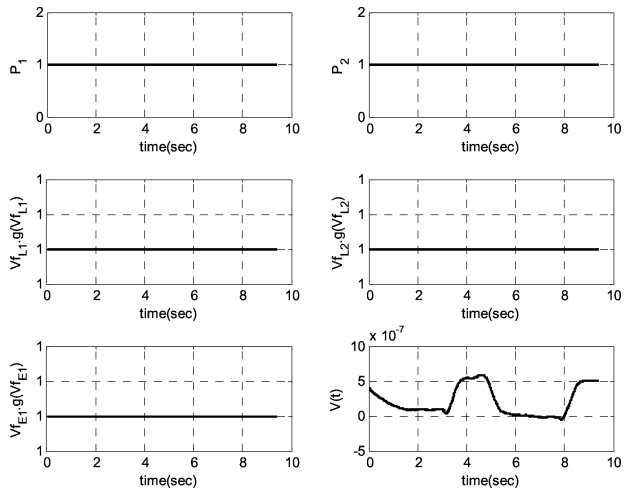


Fig. 12. Experimental results when all flywheels are on. Force and position tracking are expected to be satisfactory

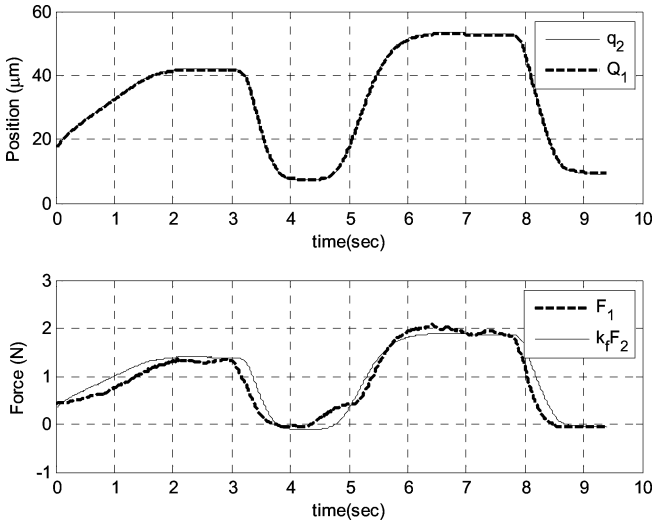


Fig. 13. Experimental results when all flywheels are on. Force and position tracking are satisfactory. After 8 μm, contact at the slave side occurs.

## 10. Experimental Results

Sampling time during experiments was chosen to be 100 μs (i.e. $1.0 \times 10^{-4}$). Saturation functions were designed in front of the master and slave control signals. These saturation functions do not permit control laws to damage the hardware. Meanwhile, sensors output signals are satisfactorily filtered (low-pass filters with a cut frequency of 20, all designed in MATLAB/Simulink). These low-pass filters are used as well in front of the velocity signals (i.e. $\dot{Q}_1$, $\dot{q}_2$) generated from direct derivation of position signals.

During experiment, some of the control gains were tuned a bit different from those of simulation (Table IV). Other parameters were kept exactly the same as simulation (Table V).

Although $T_L$ and $T_E$ are responsible for position and force tracking, it is almost correct to say that so are the master and slave controllers $T_1$ and $T_2$ ($T_L \approx T_1$, $T_E \approx T_2$). It can be checked easily by finding $S^{-T}$ arrays and then finding $T_1$ and $T_2$.

https://doi.org/10.1017/S0263574709990336 Published online by Cambridge University Press

During experiment, it was observed that at the beginning of running the controllers (i.e. before position coordination occurs), the force tracking controller $T_L$ ($\approx T_1$, based on the discussion above) signal is very large. It is so, since $T_L$ includes $q_E$ and $\dot{q}_E$ terms within itself. This large master control signal can easily damage the hardware. To cope with this issue, $q_E$ and $\dot{q}_E$ terms were omitted from $T_1$:

$$T_1(t) = T_1^{\text{old}}(t) - (-K_v\dot{q}_E - K_p q_E + \hat{B}_E\dot{q}_E), \qquad (49)$$

where $T_1^{\text{old}}(t)$ is the signal exited from $S^{-T}$ (Fig. 5).

As illustrated in Fig. 12, all flywheels (shape and locked) are turned on and their speeds do not drop below the thresholds. Therefore, according to Theorems 5.2 and 5.3, satisfactory position and force tracking are expected. Figure 13 confirms this anticipation. Also, the system is robustly stable.

## 11. Conclusions

In this research, a 1-DOF force reflecting tele-micromanipulation system was designed, experimentally implemented, and controlled. This system enabled the human operator to precisely position objects with haptic feedback. A piezo-actuator was used as the slave robot. The LuGre friction model was used to model and compensate for hysteretic behavior. A 2-DOF master–slave system (1-DOF each) was decomposed into the shape and the locked systems. For the shape system, a position tracking controller was designed in order to achieve position coordination. Also, a force tracking controller was designed for the locked system to achieve tracking of the force signals. Using these controllers, transparency was remarkably enhanced. The simulation and experimental results confirmed the following: (1) capability of the proposed control architectures to keep stability while enhancing transparency; (2) the LuGre model successfully compensating for hysteretic nonlinearity.

This research was focused on a 1-DOF macro–micro telemanipulation system. Generalizing this control architecture to the system of higher degree of freedom (with higher degree of freedom master and/or slave) may be a title for the future researches. In fact, the topic is interesting since modeling and compensation of a multi-DOF piezo-actuator is much more complicated, developing new issues to deal with.[11]

Time delay in communication channels was assumed to be negligible (below 0.1 s)[30] due to adequately high sampling rate of the experimental apparatus. Thus, considering time delay for this control framework will remain another title for future works.

## References


1. A. Kawaji, F. Arai and T. Fukuda, "Calibration for contact type of micro-manipulation," *Proc. 1999 IEEE/RSJ Intern. Conf. Intelligent Robotic*, Kyongju, Korea (1999).
2. S. Yu and B. J. Nelson, *Microrobotic Cell Injection* (IROS, Seoul, Korea, 2001) pp. 620–625.
3. A. Bergander, J. M. Breguet, R. Perez and R. Clavel, "PZT based manipulators for cell biology," *Int. Symp. Micromechatronics and Human Science*, Nagoya, Japan (2001) pp. 193–196.
4. F. J. Lin, H. J. Shieh and P. K. Huang, "Adaptive wavelet neural network control with hysteresis estimation for piezo-positioning mechanism," *IEEE Trans. Neural Networks* **17**(2) (Mar. 2006).
5. D. Mayergoyz, "Dynamic preisach models of hysteresis," *IEEE Trans. Magn.* **24**(6), 2925–2927 (Nov. 1988).
6. A. Reimers and E. D. Torre, "Fast preisach-based magnetization model and fast inverse hysteresis model," *IEEE Trans. Magn.* **34**(6), 3857–3866 (Nov. 1998).
7. D. Song and C. J. Li, "Modeling of piezo actuator's nonlinear and frequency dependent dynamics," *Mechatronics* **9**, 391–410 (1999).
8. S. Mittal and C. H. Menq, "Hysteresis compensation in electromagnetic actuators through preisach model inversion," *IEEE/ASME Trans. Mechatron.* **5**(4), 394–409 (Dec. 2000).
9. J. J. Tzen, S. L. Jeng and W. H. Chieng, "Modeling of piezoelectric actuator for compensation and controller design," *Precision Eng.* **27**, 70–86 (Jan. 2003).
10. H.-J. Shieh, F.-J. Lin, P.-K. Huang and L.-T. Teng, "Adaptive displacement control with hysteresis modeling for piezoactuated positioning mechanism," *IEEE Trans. Industr. Electr.* **53**(3), 905–914 (June 2006).
11. F. J. Lin, H. J. Shieh, P. K. Huang and P.-H. Shieh, "An adaptive recurrent radial basis function network tracking controller for a two-dimensional piezo-positioning stage," *IEEE Trans. Ultrasonics, Ferroelectrics Frequency Control* **55**, 183–198 (2008).
12. D. A. Lawrence (1992), "Stability and transparency in bilateral teleoperation," *IEEE Trans. Robot. Autom.* **9**(5), 625–637 (1992).
13. Y. Yokokohji and T. Yoshikawa, "Bilateral control of master–slave manipulators for ideal kinesthetic coupling-formulation and experiment," *IEEE Trans. Robot. Autom.* **10**(5), 605–620 (1994).
14. P. Y. Li, "Passive control of bilateral teleoperated manipulators," *Proc. American Control Conference*. (Philadelphia, 1998) pp. 3838–3842.
15. D. Lee and P. Y. Li, "Passive bilateral control and tool dynamics rendering for nonlinear mechanical teleoperators," *IEEE Trans. Robot.* **21**(5), 936–951 (Oct. 2005).
16. D. Lee and P. Y. Li, "Passive bilateral feedforward control of linear dynamically similar teleoperated manipulators," *IEEE Trans. Robot.* **19**(3), 443–456 (Jun. 2003).
17. R. Seifabadi, S. M. Rezaei and S. Shiry, "Robust impedance control of a delayed telemanipulator considering hysteresis nonlinearity of the piezo-actuated slave robot," *EuroHaptics* 2008, LNCS 5024 (2008) pp. 63–72.
18. M. Boukhnifer and A. Ferreira, "$H_\infty$ Loop shaping bilateral controller for a two-fingered tele-micromanipulation system," *IEEE Trans. Control Syst. Technol.* **15**(5), 891–905 (Sep. 2007).
19. P. Y. Li and R. Horowitz, "Passive velocity field control of mechanical manipulators," *IEEE Trans. Robot.* **15**(4), 751–763 (Aug. 1999).
20. K. Ogata, *Modern Control Engineering*, 3rd ed. (Prentice Hall, US, 1990).
21. C. Canudas de wit, H. Olsson, K. Astom and P. Lischinsky, "A new model for control of systems with friction," *IEEE Trans. Autom. Control* **40**(3), 419–425 (Mar. 1995).
22. M. Gafvert, Comparison of Two Friction Model, *Master Thesis* (Automatic Control Department, Lunde Institute of Technology, 1996).
23. K. Kuhnen and H. Janocha, "Complex hysteresis modeling of a broad class of hysteretic nonlinearities," *Proc. 8th Int. Conf New Achraiors*, Bremen (Jun. 2002) pp. 688–691.
24. H. Habibollahi, M. Rezaei, S. S. Ghidary, M. Zareinejad, R. Seifabadi and K. Razi, "Multirate prediction control of piezoelectric actuators," *IFAC*, Seoul, South Korea (2008).


https://doi.org/10.1017/S0263574709990336 Published online by Cambridge University Press

25. H. Habibollahi, M. Rezaei, S. S. Ghidary, M. Zareinejad, K. Razi and R. Seifabadi, "Hysteresis compensation of piezoelectric actuators under dynamic load condition," *IROS*, San Diego, CA (2007).
26. Y. Wang, Z. Xiong, H. Ding and X. Zhu, "Nonlinear friction compensation and disturbance observer for a high-speed motion platform," *Proc. 2004 IEEE Int. Conf. Robotics 6. Automation*, New Orleans, LA (Apr. 2004).
27. D. Tan, Y. Wang and L. Zhang, "Reserch on the parameter identification of LuGre tire model based on genetic algorithm," *ISKE-2007 Proc.* Berlin (Oct. 2007).
28. R. Seifabadi, Modeling of a Teleoperation System with Piezo-Actuator for Micromanipulation, *Master Thesis* (Mechanical Engineering Department, Amirkabir University of Technology (Tehran Polytechnic), 2008) pp. 83–84, 118.
29. N. Barabanov and R. Ortega, "Necessary and sufficient conditions for passivity of the LuGre friction model," *IEEE Trans. Autom. Control* **45**(4), 830–832 (Apr. 2000).
30. G. Niemeyer, Using Wave Variables in Time Delayed Force Reflecting Teleoperation, *Ph.D. Thesis* (Department of Aeronautics and Astronautics, Massachusetts Institute of Technology, 1996) pp. 269–281.
31. D. J. Lee and M. N. Spong, "Passive bilateral teleoperation with constant time delay," *IEEE Trans. Robot.* **22**(2) (Apr. 2006).

https://doi.org/10.1017/S0263574709990336 Published online by Cambridge University Press